

## **Back-to-back occurrence of tropical cyclones in the Arabian Sea during October-November 2015: Causes and responses**

**Riyanka Roy Chowdhury<sup>1</sup>, S. Prasanna Kumar<sup>2\*</sup>, Jayu Narvekar<sup>2</sup>, Arun Chakraborty<sup>1</sup>**

<sup>1</sup>Centre for Oceans, Rivers, Atmosphere and Land Sciences, Indian Institute of Technology Kharagpur, Kharagpur 721302, West Bengal, India

<sup>2</sup>CSIR-National Institute of Oceanography Dona Paula, Goa-403 004, India

\*Corresponding author: S. Prasanna Kumar ([prasanna.ocean@gmail.com](mailto:prasanna.ocean@gmail.com))

### **Abstract**

In the Arabian Sea, two extremely severe cyclonic storms occurred back-to-back during October-November 2015. Using a suite of ocean and atmospheric data we examined the upper ocean responses of tropical cyclones Chapala and Megh, the latter originated immediately after the dissipation of the former. Cyclones Chapala and Megh cooled the sea surface by 1.5°C and 1.0°C respectively, which was also captured by Bio-Argo float in the vicinity of their tracks. The cyclone-induced chlorophyll-a enhancement was 6 and 2 times respectively from their pre-cyclone value of 0.36 and 0.30 mg/m<sup>3</sup>, while the net primary productivity showed an increase of 5.8 and 1.7 times respectively from the pre-cyclone values of 496.26 and 518.63 mg C m<sup>-2</sup> day<sup>-1</sup> after the passage of Chapala and Megh. The CO<sub>2</sub> flux showed a 6-fold and 2-fold increase respectively compared to the pre-cyclone value of 2.69-3.58 and 6.78 mmol m<sup>-2</sup> day<sup>-1</sup>. We show that the anomalous co-occurrence of the positive phase of Indian Ocean dipole and the strong El Niño supported large-scale warming in the western Arabian Sea. Subsequent altered Walker-circulation played a decisive role in the pre-conditioning of both atmosphere and ocean, which led to a situation congenial for cyclogenesis. What triggered the formation of the cyclone Chapala was the arrival of eastward propagating atmospheric convection associated with the Madden-Julian Oscillation. The generation of the second cyclone Megh within eight-days appears to be associated with the oceanic Rossby wave that led to an increase in the upper-ocean heat content by deepening the 26°C isotherm in the vicinity of the origin of cyclones.

### **Plain Language Summary**

The Arabian Sea, situated in the western part of the North Indian Ocean, is prone to cyclones and it has a profound impact on its biogeochemistry. It is in this context that our study is important as it aims at understanding the response of the back-to-back cyclones Chapala and Megh that occurred during October-November 2015 which is a rare phenomenon. Rare because once a cyclone is generated it utilizes the available heat energy of the upper ocean and hence another cyclone cannot be formed immediately in the same region. Through this study, we show that in October-November 2015 an unusual warming occurred in the western Arabian Sea due to a unique co-occurrence of an ocean-atmosphere condition that favored the formation of back-to-back cyclones. Our study shows that the twin cyclones Chapala and Megh increased the biological productivity of the ocean as well as the emission of CO<sub>2</sub> gas from ocean to atmosphere 2 to 6 times. The implication of our result is that if the number of cyclones is going to increase in the future Arabian Sea will become oxygen deficit and it will give out more CO<sub>2</sub> to the atmosphere thereby increasing the chance of more warming.

**Keywords:** SST cooling; Tropical cyclone heat potential; Relative vorticity; Ekman pumping velocity; Net primary productivity; CO<sub>2</sub> out-gassing; Madden Julian Oscillation; Rossby Wave; Indian Ocean dipole; El Niño.

## 1. Introduction

Arabian Sea (AS) is a tropical ocean basin situated in the western part of the north Indian Ocean (NIO). The northern part of this ocean basin is landlocked at approximately 25°N. It is influenced by semi-annually reversing monsoon wind systems, namely, the summer/southwest monsoon (SWM) from June to September and winter/northeast monsoon (NEM) from November to February. During both the monsoons the winds are highly organized and largely unidirectional over the AS, though the summer monsoon winds are three-times stronger than that of the winter monsoon. Between these monsoons, the spring (March-April-May) and fall (October) intermonsoons are characterized by weak and variable winds over the AS. Apart from the above distinctions, the AS has several unique features. Biologically it is one of the most productive regions of the world oceans (Ryther et al. 1966). The high primary productivity of the AS is contributed by the phytoplankton blooms that occur during both monsoons. In the summer monsoon the coastal upwelling along Somalia, Arabia and southern part of the west coast of India (Smith and Bottero, 1977; Sharma, 1978; Smith and Codispoti, 1980; Banse, 1987; Brock and McClain, 1992) as well as the open ocean upwelling (Bauer et al., 1991; Prasanna Kumar et al., 2001a), driven by curl of the wind stress north of the Findlater Jet (Findlater, 1969), make the AS productive. During winter monsoon the cooling-driven convective mixing initiates the phytoplankton bloom in the northern part of the AS (Prasanna Kumar and Prasad, 1996; Madhupratap et al., 1996; Prasanna Kumar et al., 2001b). The huge amount of sinking organic carbon, arising due to high primary productivity, combined with slow advection of oxygen-rich water from south of equator leads to the formation of a mid-depth (150-1000 m) oxygen minimum zone (OMZ) in the AS (Morrison et al., 1998). Accordingly, the AS houses one of the most intense OMZ and denitrification zone (Naqvi et al., 1990; Olson et al., 1993) of the world oceans. See Fig. 1 for the geographical location of summer and winter blooms, Find later Jet and OMZ.

The AS is also a site of tropical cyclones that occur during spring-summer (May- June) and fall-winter (October- November) transition periods. However, the ratio of occurrence of tropical cyclones in the AS is four times lesser (Dube et al., 1997) than that in the Bay of Bengal located in the eastern part of the NIO. Though the number of the tropical cyclone is less, its impact on the AS biogeochemistry is huge. For example, an increase in the production of organic carbon mediated by the cyclone-induced phytoplankton bloom (Subrahmanyam et al., 2002; Naik et al., 2008; Piontkovski et al., 2010; Byju and Prasanna Kumar, 2011) will exert additional pressure on the already existing OMZ due to increase in the demand of oxygen. This will lead to an intensification of

denitrification which has the potential for the production of nitrous oxide, a potent greenhouse gas. Similarly, tropical cyclone leads to the out-gassing of CO<sub>2</sub> from ocean to atmosphere, as it brings subsurface cold water abundant in dissolved CO<sub>2</sub> to the warm upper ocean. Since the AS is already a perennial source of CO<sub>2</sub> with an annual flux of 47 terra gram (Goyet et al., 1998; Sarma et al., 1998 & 2003; Sabine et al., 2000), this additional CO<sub>2</sub> flux associated with tropical cyclones from ocean to atmosphere will make the AS a much stronger source.

There have been several earlier studies on tropical cyclones in the AS addressing various aspects such as sea surface cooling and air-sea interaction, prediction of cyclone track and intensity, and enhancement of chlorophyll and biological productivity. Murty et al. (1983) were the first to study the impact of cyclone in the AS. They reported a decrease of 1.2° C in the sea surface temperature (SST) in the east-central region during 14-18 June 1979. Using data from met-ocean buoys Premkumar et al. (2000) showed an abrupt drop of SST by 3° C due to the passage of tropical cyclone during 5-8 June 2008. Subrahmanyam et al. (2002) documented the enhancement of satellite-derived chlorophyll-a (Chl-a) concentrations in the range of 5 to 8 mg/m<sup>3</sup> in the east-central AS during 21-28 May 2001 associated with the cyclone. Based on shipboard measurements Naik et al. (2008) showed a drop of SST by 4° C and Chl-a enhancement of 4 mg/m<sup>3</sup>. Associated with the cyclone Phyan during 8-11 November 2009, Byju and Prasanna Kumar (2011) noticed a decrease of SST by 2° C and enhancement of Chl-a by 1.5 mg/m<sup>3</sup>. They also estimated the CO<sub>2</sub> flux to the atmosphere associated with the cyclone to be 0.123 Tg C. The climatology of the AS cyclonic storm had been analysed by Evan and Camargo (2011) and suggested that May and June's storms were associated with early and late-onset of southwest monsoon respectively. More recently Muni Krishna (2016) observed a 6°C cooling of SST due to the passage of cyclone Phet which deepened the mixed layer by 79 m and thermocline displacement by 13 m.

Recent studies have shown that the western tropical Indian Ocean including AS is warming at a rate faster than the rest of the tropical oceans (Roxy et al., 2014; 2015). In a warming environment, the frequency and intensity of tropical cyclones are likely to increase (Trenberth, 2005; Emanuel, 2005; Webster et al., 2006). For example, Yu and Wang (2009) based on ensemble simulations from 15 coupled general circulation models, using a doubled CO<sub>2</sub> concentration, showed a 4.6% increase in the tropical cyclone potential intensity over the AS. Based on tropical cyclone data from 1970 to 2007, Prasanna Kumar et al. (2009) reported a five-fold increase in the occurrence of tropical cyclone after 1995, a period when the AS was undergoing a regional climate shift. Subsequently, Evan and Camargo (2011) proposed that the recent increase in the intensity of pre-monsoon (May-

June) tropical cyclones in the AS is a consequence of the reduction in the basin-wide vertical wind shear due to the simultaneous increase in the anthropogenic black carbon and sulphate emission.

Thus, it is clearly evident from the above that the study on the tropical cyclones in the AS has special significance due to its potential impact on OMZ and regional CO<sub>2</sub> balance. Though there exists an adequate understanding of upper ocean response to a tropical cyclone in the AS in terms of air-sea interaction and cooling of SST, our understanding of cyclone induced biogeochemical changes is meager. Hence, there is a need for more studies focusing on the impact of cyclones on the biogeochemistry of the AS. This is the motivation of present study in which we examined (1) the back-to-back occurrence and evolution of tropical cyclones Chapala and Megh in the AS during October-November 2015, (2) cyclone-induced upper ocean response in terms of SST cooling, biological productivity and CO<sub>2</sub> out-gassing, and (3) the probable causes that triggered the formation of both cyclones. We wish to point out that back-to-back occurrence of tropical cyclones is a special case because when a region generates a tropical cyclone it consumes the available oceanic heat content of the upper ocean for its genesis and subsequent evolution. Hence, the region is generally unable to support the formation of another tropical cyclone immediately. However, in 2015 two tropical cyclones Chapala and Megh occurred in the AS one after the other during October-November, which is unusual.

## **2. Data and Methods**

### **2.1 Physical parameters**

Several in situ, as well as remote sensing data pertaining to both oceanic and atmospheric parameters, were used for the present study. The information on the cyclones Chapala and Megh were taken from Indian Meteorological Department (IMD) best tracks data ([http://www.rsmcnewdelhi.imd.gov.in/index.php?option=com\\_content&view=article&id=48&Itemid=194&lang=en](http://www.rsmcnewdelhi.imd.gov.in/index.php?option=com_content&view=article&id=48&Itemid=194&lang=en)). The daily sea surface temperature (SST) during 24<sup>th</sup> October to 14<sup>th</sup> November 2015 were extracted from National Oceanic and Atmospheric Administration (NOAA) high-resolution blended analysis of daily SST (Reynolds et al., 2007) downloaded from Asia-Pacific Data-Research center (APDRC) having a spatial resolution of 0.25 degree (<http://apdrc.soest.hawaii.edu/las/v6/constrain?var=1234>) for along-track time evolution associated with the life cycle of two cyclones, while the monthly mean SST for the period 1979 to 2017 were obtained from NOAA SST (Huang et al. 2017)

(<http://apdrc.soest.hawaii.edu/las/v6/constrain?var=1234/>), which is a blended product of extended reconstructed SST (ERSST) and Optimum Interpolation SST (OISST). The monthly mean SST data were further used for the calculation of monthly mean climatology. The information on IOD (Saji et al., 1999) and El Niño years were obtained from the websites <http://www.bom.gov.au/climate/iod/> and <https://ggweather.com/enso/oni.htm> respectively. Daily sea level anomaly (SLA), having a spatial resolution of 0.25 degree latitude by longitude, was taken from Copernicus Marine Environment Monitoring Services (CMEMS)

([http://marine.copernicus.eu/services-portfolio/access-to-products/?option=com\\_csw&view=details&product\\_id=SEALEVEL\\_GLO\\_PHY\\_L4\\_REP\\_OBSERVATIONS\\_008\\_047](http://marine.copernicus.eu/services-portfolio/access-to-products/?option=com_csw&view=details&product_id=SEALEVEL_GLO_PHY_L4_REP_OBSERVATIONS_008_047)).

The daily zonal and meridional surface wind components at 10 m height having a spatial resolution of 0.25 degree latitude by longitude were obtained from the advanced scatterometer (ASCAT) level 3 products

(<http://apdrc.soest.hawaii.edu/las/v6/dataset?catitem=12664>). This has been further used for the calculation of along-track wind speed (magnitude of the resultant wind), wind stress curl and Ekman pumping velocity (Gill, 1982) as detailed below:

$$\text{Windstresscurl} = \frac{\partial \tau_y}{\partial x} - \frac{\partial \tau_x}{\partial y} [1]$$

$$\text{Ekmanpumpingvelocity} = \frac{-1}{\rho f} \left( \frac{\partial \tau_y}{\partial x} - \frac{\partial \tau_x}{\partial y} \right) [2]$$

Where  $\tau_x$  and  $\tau_y$  are the zonal and meridional wind stress components,  $\rho$  is the density of seawater and its value is taken as  $1026 \text{ kg m}^{-3}$ , and  $f$  is the Coriolis parameter. Seasonal mean climatology of wind data at 10 m depth was taken from National Centers for Environmental Prediction (NCEP) reanalysis (<https://www.esrl.noaa.gov/psd/data/gridded/data.ncep.reanalysis.pressure.html>).

The tropical cyclone heat potential (TCHP) and oceanic heat content (OHC) in the upper 300 m, can be calculated using the following equations [3] and [4]. In the present study, we have downloaded the TCHP and OHC data from the climate forecast system reanalysis (CFSR) of National Centre for Environmental Prediction (NCEP) climate forecast system version 2 (Saha et al., 2014). The TCHP and OHC datasets were downloaded from APDRC Live Access Server (<http://apdrc.soest.hawaii.edu/las/v6/constrain?var=3227>)(<http://apdrc.soest.hawaii.edu/las/v6/constrain?var=3059>).

$$TCHP = \rho c_p \int_0^{D_{26}} [T(z) - 26] dz [3]$$

$$OHC = \rho c_p \int_{h_2}^{h_1} T(z) dz [4]$$

Where  $\rho$  is the density of seawater,  $c_p$  is the specific heat capacity of seawater,  $D_{26}$  is the depth of 26°C isotherm,  $h_1$  and  $h_2$  are the lower and upper water depths, and  $T(z)$  is the temperature profile.

The daily temperature profile was taken from Hybrid Coordinate Ocean Model (HYCOM) global 1/12 degree reanalysis data product ([http://apdrc.soest.hawaii.edu/las\\_ofes/v6/constrain?var=237](http://apdrc.soest.hawaii.edu/las_ofes/v6/constrain?var=237)) for the period from 2014 to 2015 to calculate the monthly mean  $D_{26}$  for deciphering its time evolution in the context of SLA variability. The 6-hourly sea level pressure (SLP) data were taken from Fleet Numerical Meteorology and Oceanography Centre (FNMOC) having a spatial resolution of one degree and converted into daily data

(<https://coastwatch.pfeg.noaa.gov/erddap/griddap/erdlasFnPres6.html>).

To decipher the time evolution of vertical profiles of temperature, salinity, and chlorophyll-*a*, in the upper water column in response to the passage of cyclone Chapala and Megh, we have analyzed the trajectory of Argo/Bio-Argo that were in the vicinity of the track of the tropical cyclone (Fig. 2). We could identify a Bio-Argo with ID-2902120 (Green filled circles in Fig. 2) located near the origin of both cyclones. The Argo data were downloaded from the Argo CORIOLIS site (<http://www.coriolis.eu.org/Data-Products/Data-Delivery/Data-selection>). The mixed layer depth (MLD) was calculated following Monterey and Levitus (1997), while isothermal layer depth (ILD) was calculated as the depth at which the temperature decreases by 0.5°C from the SST.

In order to gain an insight into the atmospheric parameters that are crucial for the formation and development of tropical cyclone we have computed the relative vorticity using the following equation

$$Relative\ vorticity = \frac{\partial v}{\partial x} - \frac{\partial u}{\partial y} \quad [5]$$

where  $v$  = meridional wind component at 850 hPa and  $u$  = zonal wind component at 850 hPa. The zonal and meridional components of hourly wind at 0.5° spatial resolution were downloaded from CFSR of NCEP climate forecast system (<http://apdrc.soest.hawaii.edu/las/v6/dataset?catitem=3007>) version 2 (Saha et al., 2014). Hourly wind data converted to daily and was further used for the computation of vertical wind shear between 200 and 850 hPa following Evan and Camargo (2011) and Balaji et al. (2018). The daily data on

relative humidity at 500 hPa was taken from NCEP 2 reanalysis (Kalnay et al., 1996) having a spatial resolution of 2.5 degree latitude by longitude (<https://www.esrl.noaa.gov/psd/data/gridded/data.ncep.html>).

The daily Outgoing Long wave Radiation (OLR) data for the period 1979 to 2017 were obtained from NOAA (Liebmann and Smith, 1996) (<https://www.ncei.noaa.gov/data/outgoing-longwave-radiation-daily/access/>), which has been subjected to Morlet wavelet power spectrum analysis (for details see Torrence and Compo, 1998; Torrence and Webster, 1999; Grinsted et al., 2004) to decipher the dominant periodicities present in the data. Further, the daily OLR data, as well as data on zonal wind at 850 hPa, was subjected to a five-day running mean for the period 1<sup>st</sup> May to 31<sup>st</sup> December 2015 to decipher the presence of Madden-Julian Oscillation (MJO) signal during the period of cyclones.

## 2.2 Biological parameters

The satellite-derived 3-day composite values of surface chlorophyll-a (Chl-a) pigment concentration were computed from the daily data taken from Moderate Resolution Imaging Spectroradiometer (MODIS) Aqua Ocean color ([https://oceandata.sci.gsfc.nasa.gov/MODIS-Aqua/Mapped/Daily/4km/chlor\\_a/](https://oceandata.sci.gsfc.nasa.gov/MODIS-Aqua/Mapped/Daily/4km/chlor_a/)). The Level 3 Chl-a dataset has a zonal and meridional resolution of 0.04-degree longitude by latitude. The monthly mean Chl-a climatology data were taken from National Aeronautics and Space Administration (NASA) ocean color data having a spatial resolution of 9 km ([https://oceandata.sci.gsfc.nasa.gov/SeaWiFS/Mapped/Monthly\\_Climatology/9km/chlor\\_a/](https://oceandata.sci.gsfc.nasa.gov/SeaWiFS/Mapped/Monthly_Climatology/9km/chlor_a/)) for the computation of seasonal mean climatology for the period from June to August. The vertically generalized productivity model (VGPM) has been utilized for the estimation of net primary production (NPP) following Behrenfeld and Falkowski (1997). The NPP data was taken from MODIS Aqua Ocean color (<https://coastwatch.pfeg.noaa.gov/erddap/griddap/erdMH1pp1day.html>).

## 2.3 CO<sub>2</sub> flux

To determine the net CO<sub>2</sub> flux along the track of the Chapala and Megh, before, during, and after its passage, the pCO<sub>2</sub><sup>air</sup> data was taken from NOAA ESRL ([ftp://aftp.cmdl.noaa.gov/product/trends/co2/co2\\_mm\\_g1.txt](ftp://aftp.cmdl.noaa.gov/product/trends/co2/co2_mm_g1.txt)). As the daily pCO<sub>2</sub><sup>sea</sup> values are not available, the climatological pCO<sub>2</sub><sup>sea</sup> values were calculated from Joint Global Ocean Flux Studies (JGOFS) Arabian Sea profiles (<http://usjgofs.whoi.edu/jg/serv/jgofs/arabian/INVENTORY.html>) using CO2SYS (Heuven et al., 2011). The net CO<sub>2</sub> flux was calculated using the following formula

$$F = k. a. (\rho CO_2^{sea} - \rho CO_2^{air}) \quad [6]$$



where  $k$  denotes the gas transfer velocity,  $a$  is the solubility of CO<sub>2</sub> in seawater which is the dependent parameter of sea surface temperature and salinity (Weiss, 1974) as per the following equations. Salinity data was taken from HYCOM global reanalysis data product ([http://apdrc.soest.hawaii.edu/las\\_ofes/v6/constrain?var=237](http://apdrc.soest.hawaii.edu/las_ofes/v6/constrain?var=237)).

$$\ln a = A_1 + A_2 \left( \frac{100}{T} \right) + A_3 \ln \left( \frac{T}{100} \right) + S \left[ B_1 + B_2 \left( \frac{T}{100} \right) + B_3 \left( \frac{T}{100} \right)^2 \right] \quad [7]$$

The gas transfer velocity “ $k$ ” was calculated following Wanninkhof (1992)

$$k(\text{cmh}^{-1}) = \Gamma U^2 \left( \frac{S_c}{660} \right)^{-1/2} \quad [8]$$

where  $\Gamma$  is the scaling factor and its value of 0.26 is taken from Takahashi et al. (2009), while  $U$  is the wind speed.  $S_c$  is the Schmidt number (ratio of kinematic viscosity of water to diffusion coefficient of CO<sub>2</sub> in water), the value of which is 660 for CO<sub>2</sub> in seawater at 20°C which is a function of temperature and is computed using the following formula

$$S_c = A - BT + CT^2 - DT^3 \quad [9]$$

For the values of the constants A, B, C, and D refer Weiss (1974) and Wanninkhof (1992).

### 3. Life cycle of cyclones Chapala and Megh

As per the Indian Daily Weather Report of India Meteorological Department (IMD) (<http://www.rsmcnewdelhi.imd.gov.in/images/pdf/publications/preliminary-report/chap.pdf>) an extremely severe cyclonic storm (ESCS) Chapala, a category-4 cyclone (Saffir-Simpson scale), originated as a low-pressure area over the southeastern AS (Fig. 2), which developed into a depression in the morning of 28<sup>th</sup> October 2015. It moved in a north-northwestward direction and intensified into a deep depression (DD) on the same evening. In the early hours of 29<sup>th</sup>, it intensified into a cyclonic storm (CS) which was named Chapala by IMD. As it moved further west-northwestward, it progressively intensified into a severe cyclonic storm (SCS), later into a very severe cyclonic storm (VSCS) and finally into an ESCS in the morning of 30<sup>th</sup>. While the system was rapidly intensifying from CS to ESCS, the surface wind speed increased from 35 kts (65 kmph) on 29<sup>th</sup> to 115 kts (213 kmph) at 0900 on 30<sup>th</sup> October. The system maintained its intensity while moving westwards until 2<sup>nd</sup> November with a surface wind speed of 100 kts (185 kmph). Thereafter while moving further westward it started weakening into VSCS and crossed Yemen coast to the southwest of Riyan (14.1°N and 48.65°E) in the early hours of 3<sup>rd</sup> November 2015 with a maximum surface wind speed of 65 kts (120 kmph). As it moved further westward, it rapidly weakened from



SCS to depression and finally to well-marked low pressure over Yemen in the early hours of 4<sup>th</sup> November 2015. The system travelled a distance of about 2250 km during its life period.

Interestingly, eight days after the formation of cyclone Chapala, another depression formed over the east-central AS in the early hours of 5<sup>th</sup> November (Fig. 2b) which was just 2.6° north of and 1.0° east of the origin of Chapala. The depression moved in a westwards/west-southwestwards direction to intensify into a DD and subsequently by noon when it turned into CS, a category-3 cyclone (Saffir-Simpson scale), it was named Megh by IMD. It continued its west-southwestward movement at a rather slow rate maintaining a wind speed of 45 kts (83 kmph), which intensified into SCS only on 7<sup>th</sup> November at 0600 UTC. At 1500 UTC it turned into a VSCS and later into ESCS at 0300 UTC of 8<sup>th</sup> November with a wind speed of 90 kts (167 kmph). Maintaining its peak wind speed of 95 kts (176 kmph) for a short period of about 6 hrs it moved west-northwestward and gradually weakened into a VSCS at 0000 UTC and SCS at 2100 UTC of 9<sup>th</sup> November. The system further weakened into a CS at 0300 UTC of 10<sup>th</sup> and finally into a DD at 0600 UTC of 10<sup>th</sup> November. At 0900 UTC of 10<sup>th</sup> it crossed Yemen coast near 13.4°N and 46.1°E as a DD. Continuing its west-northwest movement it weakened into a depression at 1200 UTC of 10<sup>th</sup> November 2015. The system travelled a distance of about 2307 km during its life period.

Thus, (1) the back-to-back occurrence of a category-4 tropical cyclone Chapala (28<sup>th</sup> October to 4<sup>th</sup> November) and a category-3 tropical cyclone Megh (5<sup>th</sup> to 10<sup>th</sup> November) within eight days, and (2) the proximity of the region of origin of both cyclones made the cyclones exceptional.

#### **4.Upper ocean response**

In order to decipher the upper ocean response due to back-to-back occurrence of the cyclones Chapala and Megh, we analyzed the time evolution of physical parameters, CO<sub>2</sub> flux, and biological parameters, along the tracks of both the cyclones. For along the track calculation, we have computed the values of each parameter at 3-hourly position of the cyclone along the track, keeping the position of the cyclone in the center of a half-degree longitude by half-degree latitude box, and averaging these values to obtain daily mean values.

##### **4.1 Along Track Variation of physical parameters**

At first, we examined the along-track variation of tropical cyclone heat potential (TCHP, KJ/m<sup>2</sup>) that provides the heat energy for the generation of the cyclone, and the sea surface temperature (SST, °C) which indicates the response of the upper ocean to the cyclone. We also examined Ekman pumping velocity (EKV, m/day, upward positive and downward negative), as it would potentially cool the SST by bringing subsurface waters to the ocean surface. All the above parameters were analyzed

before, during, and after the passage of cyclones, that is from 24<sup>th</sup> October to 14<sup>th</sup> November 2015 for Chapala (Fig. 3a solid lines) and for Megh (Fig. 3a broken lines). The TCHP showed a monotonic decrease during and after the cyclone Chapala (Fig. 3a solid line). However, the rate of decrease was not uniform throughout the study period. From 27<sup>th</sup> to 31<sup>st</sup> October when the low pressure over the southeastern AS intensified into ESCS, the TCHP showed a slow decrease of  $0.2 \times 10^8 \text{ kJ/m}^2$ . In contrast, when the system was maintaining its intensity until 2<sup>nd</sup> November, and finally dissipated on 4<sup>th</sup> November the TCHP showed a rapid decrease of  $0.8 \times 10^8 \text{ kJ/m}^2$ . This rapid decrease continued until 6<sup>th</sup> November, much beyond the cyclone period, losing another  $0.5 \times 10^8 \text{ kJ/m}^2$ . The overall decrease of TCHP during the cyclone Chapala period (shaded region in Fig.3a) was consistent with SST, which also showed an overall decrease of  $1.5^\circ\text{C}$ , from its pre-cyclone value. Similar to the TCHP, SST showed a slow decrease of  $0.5^\circ\text{C}$  during the intensification phase of Chapala and a rapid decrease of  $1.0^\circ\text{C}$  during the decay phase. This pattern of differential decrease in both TCHP and SST could be explained as follows. As the low-pressure system develops into a category-4 cyclone Chapala, the heat energy stored in the upper ocean, generally enclosed by the  $26^\circ\text{C}$  isotherm, is utilized. This along with the enhanced evaporation under the strengthening winds (not shown) which cools the SST (Price, 1981) would explain the initial decrease in both the parameters. In addition, during the weakening phase of the system, though the utilization of heat energy would considerably decrease, the Ekman pumping associated with the cyclonic wind would continue to bring colder waters from the subsurface to the surface of the ocean as seen from the positive values of EKV. Prior to the cyclone, the EKV was almost zero/weakly negative but showed a rapid increase reaching a maximum of  $1.2 \text{ m/day}$  on 29<sup>th</sup> October (Fig. 3a solid line) associated with the strengthening of the system. Subsequently, though the magnitude of EKV decreased, the upward Ekman pumping continued to supply colder waters to the upper ocean, thereby sustaining the cooling of the upper water column. Note that the magnitude of cooling by the upward Ekman pumping is much greater than that due to the wind-driven evaporative cooling that happens under the strong winds. During the active phase of a cyclone, the upper ocean will experience a sustained cooling due to three main processes such as oceanic vertical mixing, advection, and air-sea heat exchange. The upper-ocean cooling is primarily controlled by entrainment of cold water from the thermocline into the mixed layer. This happens through vertical mixing by the vertical shear of horizontal currents and associated upward Ekman pumping (Pollard et al., 1973; Price, 1981), which accounts for about 80% of the SST drop (Price, 1981; Sanford et al., 1987; Shay et al., 1992). The contributions by the surface heat fluxes and advection towards cooling are much lesser extent (Jacob

et al., 2000; Huang et al., 2009). This would explain the sustained rapid decrease of TCHP and SST even during the decay phase of the cyclone more rapidly.

In the case of cyclone Megh also the time evolution of TCHP and SST showed a decreasing pattern (Fig. 3a broken line), which was  $0.95 \times 10^8 \text{ kJ/m}^2$  and  $1.0^\circ\text{C}$  respectively lower than the pre-cyclone value. However, the magnitudes of decrease in both parameters were much smaller compared to that for the period of cyclone Chapala. Unlike during the period of Chapala, the rate of decrease of TCHP and SST remained approximately the same during the period of cyclone Megh. The EKV also showed an increasing trend from 2<sup>nd</sup> November, prior to the formation of the cyclone, and attained a value of 0.1 m/day on 5<sup>th</sup> November when the system intensified into a category-3 cyclone. It continued to increase reaching the highest value of 0.89 m/day on 7<sup>th</sup> November when the system further intensified into ESCS. As the system begins to weaken, the magnitude of EKV also decreased and finally reaching a negative value of 0.15 m/day indicating downward Ekman pumping velocity after the cyclone had completely dissipated. Note that the magnitudes of decrease of all the three parameters, TCHP, SST, and EKV during the cyclone Megh were much smaller compared to that for the period of cyclone Chapala. This reduction in magnitudes is linked to the upper ocean cooling after the passage of cyclone Chapala. This is also the reason why Megh was a category-3 cyclone.

#### **4.2 Along Track Variation of CO<sub>2</sub> flux**

Having examined the cyclone-induced upper ocean response of physical parameters, we now focus on the time variation of CO<sub>2</sub> flux. The basic factors that control the CO<sub>2</sub> flux from the ocean to atmosphere are (1) the wind speed which influences the gas transfer velocity at the air-sea interface, and (2) the upward Ekman pumping which brings the subsurface CO<sub>2</sub> rich cold waters to the surface leading to an increase in the gradient in partial pressure between the surface ocean and atmosphere (Bates et al., 1998). Based on a time-series data Nemeto et al. (2009) obtained a similar result from the East China Sea during the passage of a cyclone when strong wind and dissolved inorganic carbon supply from the subsurface associated with cyclone increased the out-gassing of CO<sub>2</sub> from the ocean to the atmosphere. Here we analyzed the along-track variation of CO<sub>2</sub> flux from the ocean to the atmosphere associated with Chapala (Fig.3b solid line) and Megh (Fig.3b broken line). The value of CO<sub>2</sub> flux from 24<sup>th</sup> – 25<sup>th</sup> October, much before the origin of cyclone Chapala, was in the range of  $2.69 \pm 0.02$  to  $3.58 \pm 0.05 \text{ mmol m}^{-2} \text{ day}^{-1}$ , which rapidly increased to  $13.19 \pm 0.53 \text{ mmol m}^{-2} \text{ day}^{-1}$  on 28<sup>th</sup> October (Fig.3b solid line). This continuous increase of the CO<sub>2</sub> flux from the ocean was mediated by the rapidly strengthening winds before the formation of the cyclone. During the

strengthening phase of Chapala from 28<sup>th</sup> October to 31<sup>st</sup> October when Chapala turned into ESCS, the value increased from  $13.19 \pm 0.53$  to  $19.64 \pm 0.34$   $\text{mmol m}^{-2} \text{ day}^{-1}$  which was 6-times higher than the pre-cyclone value. During the declining phase of Chapala the  $\text{CO}_2$  flux also showed a rapid decrease reaching the lowest value of  $3.64 \pm 0.01$   $\text{mmol m}^{-2} \text{ day}^{-1}$ . Thereafter, however, the  $\text{CO}_2$  flux showed an increasing trend which we infer to be the response of the strengthening winds associated with the 2<sup>nd</sup> cyclone Megh.

The  $\text{CO}_2$  flux along the track of cyclone Megh showed a decline from  $11.47 \pm 0.28$  to  $5.06 \pm 0.08$   $\text{mmol m}^{-2} \text{ day}^{-1}$  just prior to the formation of the cyclone (Fig.3b broken line). As the track of Megh was close to that of the previous cyclone Chapala, this high value of  $\text{CO}_2$  flux on 1<sup>st</sup> November 2015 was the impact of cyclone Chapala. During the period of Megh (Fig.3b broken line), however, the  $\text{CO}_2$  flux showed a rapid increase from  $6.78 \pm 0.011$   $\text{mmol m}^{-2} \text{ day}^{-1}$  on 5<sup>th</sup> November to  $13.90 \pm 0.28$   $\text{mmol m}^{-2} \text{ day}^{-1}$  on 7<sup>th</sup> November. This sudden increase of  $\text{CO}_2$  out-gassing, which was more than 2-times its immediate pre-cyclone value, was associated with the strengthening of the system to ESCS. With the dissipation of the Megh, the  $\text{CO}_2$  flux also showed a decline attaining the lowest value of  $5.15 \pm 0.09$   $\text{mmol m}^{-2} \text{ day}^{-1}$  on 10<sup>th</sup> November. Even after the dissipation of Megh, the  $\text{CO}_2$  flux showed a sustained increase after 12<sup>th</sup> November 2015, which was not linked to the cyclone response.

The above temporal variability pattern of  $\text{CO}_2$  flux could be understood in the context of the time-evolving EKV and wind (not presented). In the case of Chapala the increase in the  $\text{CO}_2$  flux during the pre-cyclone period, when the EKV was near zero or weakly negative (Fig. 3a solid line), was augmented by the increasing wind speed that enhances the gas transfer at the air-sea interface (Bates et.al.1998). Subsequently, as the strength of the cyclone increases, so does the EKV which leads to the increased levels of  $\text{CO}_2$  out-gassing compared to the initial value. Similarly, as the system decays, the EKV declines and so does the  $\text{CO}_2$  flux. The increase of  $\text{CO}_2$  flux even after the dissipation of Chapala must be linked to the increasing wind speeds associated with the formation of 2<sup>nd</sup> cyclone Megh.

In contrast, in the case of Megh, the pre-cyclone values of  $\text{CO}_2$  flux showed a decrease initially, which was consistent with the increasing value of negative EKV indicating downward Ekman pumping (Fig.3a broken line). From 2<sup>nd</sup> to 5<sup>th</sup> November, consistent with positive EKV the  $\text{CO}_2$  flux showed an increase. Subsequent strengthening of cyclone Megh and associated strengthening of upward Ekman pumping lead to the increased out-gassing of  $\text{CO}_2$ . Similarly, during the decay phase of Megh the EKV also showed a decline and  $\text{CO}_2$  flux was generally low. The increased out-gassing of  $\text{CO}_2$  after the dissipation of Megh could be explained as follows. Due to the continuous

upward Ekman pumping under the cyclonic winds during the period of both cyclones the surface ocean would accumulate large quantities of subsurface waters with a high concentration of CO<sub>2</sub>. This increases the difference in the partial pressure of CO<sub>2</sub> at the air-sea interface (Rodenbeck et al., 2013), thus leading to a continuous out-gassing, even after the dissipation of Megh. Note also the increasing trend in the EKV even after the dissipation of Megh.

In the present study, our estimate of CO<sub>2</sub> emission is in the range of 2.69±0.02 to 19.64±0.34 mmol m<sup>-2</sup> day<sup>-1</sup> associated with cyclones Chapala and Megh. These values were higher than the seasonal variability of CO<sub>2</sub> emission estimated by Sarma et al. (1998) based on the Indian Joint Global Ocean Flux Studies (JGOFS) measurements, which is in the range of 1 to 3.5 mmol m<sup>-2</sup> day<sup>-1</sup>. However, our values were much lower than those estimated by Byju and Prasanna Kumar (2011) who reported 8 mmol m<sup>-2</sup> day<sup>-1</sup> associated with cyclone Phyan during 9-11 November 2009.

#### **4.3 Along Track Variation of biological parameters**

The response time of the upper ocean to cyclone-induced changes in physical parameters and CO<sub>2</sub> flux is much less compared to biological parameters. Typical time lag associated with the chlorophyll biomass and primary production is 1 to 3 days depending upon the strength of the cyclone, its duration, and cloud coverage. Usually, due to the presence of thick cloud coverage during the cyclone period, there is a severe limitation on the availability of remote sensing data on Chl-a. Hence, it is important to establish the robustness of the satellite-derived Chl-a data before its use. Towards this, we first calculated the percentage of pixel count and Chl-a along the track of the cyclone from 3-day composite data. This is presented in figures 5 and 6 along with Chl-a for Chapala and Megh respectively. In general, the pixel count percentage showed lesser values for the period pre-cyclone to the time when cyclone undergoes intensification for both Chapala (Fig. 4a) and Megh (Fig. 4b). However, as the cyclone starts weakening the pixel count percentage showed higher values. In the case of cyclone Chapala, the pixel count percentage during the genesis and intensification phase was 5-25, while during the decay phase, it varied from 30 to 65 (Fig. 4a). For cyclone Megh, the pixel count percentage during its origin and intensification (Fig. 4b) was similar to that of Cyclone Chapala, but during decay, it varied from 15 to almost 80. This gives us enough confidence to use the 3-day composite of Chl-a data to explore the biological response due to both the cyclones.

The average Chl-a-concentration prior to the formation of cyclone Chapala was 0.36 mg/m<sup>3</sup> which increased to 0.5 mg/m<sup>3</sup> during its life cycle (28<sup>th</sup> October to 4<sup>th</sup> November) (Fig. 4a). After the decay of the cyclone, the Chl-a-concentration showed an increase in reaching the maximum value of 2.30

mg/m<sup>3</sup> on the 3-day composite centered on 5<sup>th</sup> November. This was a more than 6-fold increase from its pre-cyclone mean value. Thereafter the Chl-a concentration showed a decline reaching a value of 0.63 mg/m<sup>3</sup> on the 3-day composite centered on 11<sup>th</sup> November, which was 1.7-times higher than the pre-cyclone value, followed by an increase. In the case of Megh the pre-cyclone Chl-a concentration was in the range of 0.24 to 0.36 mg/m<sup>3</sup> (Fig. 4b) with an average value of 0.30 mg/m<sup>3</sup>, which increased to 0.61 mg/m<sup>3</sup> after the cyclone on the 3-day composite centered on 11<sup>th</sup> November. Finally, the Chl-a concentration decreased to about 0.51 mg/m<sup>3</sup> on the 3-day composite centered on 14<sup>th</sup> November. Thus, unlike the Chapala, the enhancement of Chl-a concentration associated with Megh was just 2-fold increase from its pre-cyclone value. This lower magnitude of the enhancement of chlorophyll is linked to the lower magnitude of the upward EKV associated with Megh, which was more than 1.3-fold lower in magnitude compared to Chapala.

The average NPP prior to the formation of cyclone Chapala was 496.26 mg C m<sup>-2</sup> day<sup>-1</sup> (21<sup>st</sup> to 27<sup>th</sup> October) which increased to 2883.90 mg C m<sup>-2</sup> day<sup>-1</sup> (5<sup>th</sup> to 7<sup>th</sup> November) after the decay of the cyclone on the 3-day composite centered at 5<sup>th</sup> November (Fig. 4c). This is 5.8-times more than the pre-cyclone value. Subsequently, the NPP decreased to 774.40 mg C m<sup>-2</sup> day<sup>-1</sup> (14<sup>th</sup> to 17<sup>th</sup> November), which was 1.5-times higher than the pre-cyclone value. In the case of Megh the average pre-cyclone value was 518.63 mg C m<sup>-2</sup> day<sup>-1</sup> (21<sup>st</sup> October to 9<sup>th</sup> November), which was very similar to that of Chapala. However, the post-cyclone value of NPP was 885.21 mg C m<sup>-2</sup> day<sup>-1</sup> (8<sup>th</sup> to 10<sup>th</sup> November) which was 1.7-times higher than the pre-cyclone value. Similar to that of Chl-a concentration the cyclone-induced NPP enhancement by Megh was 3-times lesser than that by Chapala.

#### **4.4 Upper ocean response captured by Argo data**

In order to compare the cyclone-induced oceanic response obtained from the satellite-derived remote sensing data with in situ data, we examined the availability of Argo profile data in the vicinity of the cyclone track. We found the Argo float with ID 2902120 was located in the south-central part of the AS, which was close to the origin of both the cyclones as indicated in Fig.2. We could obtain six vertical profiles of temperature (Fig. 5a), salinity (Fig. 5b), Chl-a (Fig. 5c) and dissolved oxygen (Fig. 5d). Of these 4 profiles, two were for October (21<sup>st</sup>, and 31<sup>st</sup>) and two for November (20<sup>th</sup>, 30<sup>th</sup>) respectively. Much before the passage of the cyclone Chapala on 21<sup>st</sup> October, the isothermal layer depth was 27 m (at 13.5°N and 64.4°E) and it progressively increased to 50 m ten days after the passage of cyclone Megh on 20<sup>th</sup> November (at 14.1°N and 63.1°E) (Fig. 5a). A surface temperature cooling of 1.5°C from 29.5°C was also noticed from 21<sup>st</sup> to 31<sup>st</sup> October associated with the passage

of Chapala, which was consistent with the magnitude of the along-track lowering of SST. The response of the upper ocean salinity to cyclone was captured by Argo profiles. Before the passage of the cyclone, salinity value was 36.15 psu on 21<sup>st</sup> October and the salinity value increased to 34.43 psu (Fig. 5b) after the passage of cyclone Megh on 20<sup>th</sup> November. A deepening of isohaline layer, broadly similar to that of the isothermal layer, was also noticed. These changes could be understood in the context of cyclone induced mixing which will deepen both isothermal and isohaline layers and increase the upper ocean salinity as the subsurface Arabian Sea high salinity water mass located in the upper halocline/thermocline mixes with surface waters. A similar deepening of the oxycline to 60 m could be noticed on 31<sup>st</sup> October (Fig. 5d) in response to mixing. The most remarkable change was noticed in the Chl-a profiles (Fig. 5c). The surface Chl-a increased from 0.1 to 1.0 mg/m<sup>3</sup>, a 10-fold increase. Similarly, the Chl-a in the subsurface chlorophyll maximum (SCM) increased from 1.5 to 2.0 mg/m<sup>3</sup>. Recall that the satellite-derived chlorophyll also showed a similar response with a 6-fold and 2-fold increase respectively after the passage of Chapala and Megh respectively.

Having examined the evolution and the response of the upper ocean to back-to-back cyclones Chapala and Megh in the AS, we now focus on to understand the ocean and atmospheric conditions that led to the genesis of both the cyclones.

### **5. Spatial distribution of ocean-atmospheric anomalies**

Environmental conditions that are necessary for the formation of a tropical cyclone are (1) SST in excess of 26°C, (2) low-level wind convergence, (3) high relative vorticity, (4) weak vertical wind shear, and (5) high relative humidity (Evan and Camargo, 2011). In order to generate low-level wind convergence, there should be enough heat in the upper ocean to create a low-pressure area.

We, therefore, have prepared spatial anomaly maps of SST, TCHP, and OHC by computing the differences between October-November 2015 value and climatological value during the period 2010 to 2016. Similarly, spatial anomaly maps of lower-tropospheric relative vorticity (850 hPa), vertical wind shear between 850 hPa and 200 hPa and mid-tropospheric relative humidity (500 hPa) were prepared by computing the differences between October-November 2015 value and climatological value during the period 2010 to 2016. The spatial anomaly patterns were analyzed in order to decipher whether the ocean-atmospheric conditions were favorable for the genesis of both the cyclones.

The spatial distribution of SST anomaly in the AS showed that the central and western AS had a positive anomaly, and the values at the origin of cyclone Chapala and Megh were 0.35°C and 0.55°C respectively higher than the climatological value (Fig. 6a). The spatial distribution of OHC anomaly also showed a region of positive value in the central and western AS, but in an elongated



patch in a southwest-northeast direction (Fig. 6b). The values within the patch were in excess of  $2 \times 10^9 \text{ K J/m}^2$  (Fig. 6b), which indicated excess the heat energy available in the upper layer of the ocean (0-300 m) during October-November 2015. The origin of both Chapala and Megh was also within the patch of high OHC anomaly. The TCHP anomaly showed a large region of high positive value in excess of  $3.0 \times 10^8 \text{ KJ/m}^2$  in the central AS (Fig. 6c). The origin of Chapala and Megh were located in a region with values  $3.5 \times 10^8 \text{ KJ/m}^2$  and  $5.5 \times 10^8 \text{ KJ/m}^2$  respectively. Thus, the anomalies of SST, OHC, and TCHP during 2015 were higher than the climatological values, indicating that the upper ocean was warmer and contained more heat energy in 2015 that could potentially spin and sustain a cyclone.

The spatial anomaly maps of lower-tropospheric relative vorticity (850 hPa) showed positive values south of  $15^\circ\text{N}$  and along the western part of the AS. The origin of Chapala and Megh were located in a region with values  $5 \times 10^{-6} \text{ s}^{-1}$  and  $3 \times 10^{-6} \text{ s}^{-1}$  respectively (Fig. 6d). On the other hand, the anomaly of vertical wind shear showed negative values south of  $17^\circ\text{N}$  with higher values towards the south (Fig. 6e). The origin of both Chapala and Megh was located within the core of the lowest wind shear with values of 3 m/s (Fig. 6e). The anomaly of mid-tropospheric relative humidity showed positive values confined to the southeastern part of the AS with the highest values towards the east (Fig. 6f). In the region of origin of both Chapala and Megh, the values during 2015 were 10% higher than that of climatology. In short, the environmental conditions in 2015 during the period October-November were favorable for the formation of cyclone in the AS with higher SST, stronger relative vorticity, weaker vertical shear, and higher relative humidity compared to the climatological values.

To understand the mechanism/processes leading to the formation of the storms, we further examined the spatial distribution of vertical shear of wind between 200 and 850 hPa, lower-tropospheric relative vorticity (850 hPa) and mid-tropospheric relative humidity (500 hPa) on 27<sup>th</sup> October 2015 (Fig. 7 left panels a,c,e) and 4<sup>th</sup> November 2015 (Fig. 7 right panels b,d,f), a day before the origin of cyclone Chapala and Megh respectively. The vertical wind shear prior to the formation of Chapala was the lowest at the location of its origin with a value between 5 and 10 m/s (Fig. 7a), while the lower-tropospheric relative vorticity and the mid-tropospheric relative humidity were high with values of  $0.75 \times 10^{-4} \text{ s}^{-1}$  (Fig. 7c) and 75% (Fig. 7e) respectively. Similarly, prior to the formation of Megh the vertical wind shear was lowest at the location of its origin with a value between 0 to 5 m/s (Fig. 7b), while the lower-tropospheric relative vorticity and the mid-tropospheric relative humidity were highest with values of  $1.5 \times 10^{-4} \text{ s}^{-1}$  (Fig. 7d) and 80% (Fig. 7f) respectively. Here again, we

see that the environmental conditions prior to the formation of both Chapala and Megh were highly favorable for cyclone formation.

Thus, from the above discussions, it is amply clear that environmental conditions in 2015 during the period October-November, in general, and prior to the genesis of both cyclones in particular, were favorable for the formation of cyclone in the AS with high SST, strong relative vorticity, weak vertical shear, and high relative humidity. The question then would be (1) what mechanism/s created the necessary ocean-atmospheric condition in 2015 that was congenial for the generation of two cyclones back-to-back and (2) what triggered the genesis?

### **6.Pre-conditioning and triggering mechanism**

To understand what created the situation congenial for the back-to-back genesis of Chapala and Megh within a week in the same region in 2015, we examined the role of climate modes such as El Niño-Southern Oscillation (ENSO) (<https://ggweather.com/enso/oni.htm>) and Indian Ocean Dipole (IOD) (<http://www.bom.gov.au/climate/iod/>) El Niño as well as positive IOD. El Niño was the strongest among those occurred during the period 1979 to 2017 (figure not shown). The co-occurrence of strongest El Niño and positive IOD makes the waters of the eastern Indian Ocean colder than normal and a region for atmospheric high pressure associated with the descending arm of the shifted Walker Circulation; while the waters in the western Indian Ocean becomes warmer than normal with atmospheric low pressure where the ascending arm of the shifted Walker Circulation originates (see Fig.12). This is amply evident from the spatial distribution of SST, sea level pressure (SLP) and sea surface wind composited for the period of both the cyclones, which showed positive (negative) SST anomaly, negative (positive) SLP anomaly and convergence (divergence) of surface wind in the western (eastern) AS indicating prevalence of warmer (colder) surface waters with low (high) pressure (Fig. 8 a,b). In order to examine the robustness of this result, we examined the spatial distribution of SST, SLP, and surface wind anomaly composited for the months of October and November 2015 (Fig. 8c,d) and also climatology (Fig. 8 e,f). The composited SST, SLP, and surface wind anomalies for October-November 2015 also showed a pattern similar to that seen during the cyclone period. In contrast, the climatology of the above parameters composited for October and November showed warm SST and low SLP in the eastern Indian Ocean and cold SST and high SLP in the western Indian Ocean which is indicative of normal Indian Ocean with ascending arm of the Walker Circulation located in the eastern Indian Ocean and descending arm in the western Indian Ocean. Thus, the high SST and the associated atmospheric convection and moisture input pre-conditioned the ocean-atmosphere in the western AS making it congenial for the formation of the

cyclone. However, these are only the necessary conditions and there needs to be a triggering mechanism that could initiate the cyclogenesis.

It is well known that in the tropical region a 30-90 days oscillation, known as Madden Julian Oscillation (MJO) (Madden and Julian, 1971 & 1972), is the primary mode of atmospheric variability in the intra-seasonal time scale. The MJO has a dominant eastward propagation during boreal winter and northward propagation during boreal summer (Zhang, 2005). This eastward-propagating atmospheric disturbance with deep convection is evident over the warm pool region from the central Indian Ocean to the western Pacific Ocean. The role of MJO in modulating the tropical cyclones over the Pacific Ocean, the Caribbean Sea (Zhang, 2005) and the Indian Ocean (Camargo et al., 2009) have been demonstrated. It also has been known that the convective phase of MJO plays a significant role in cyclogenesis (Gray, 1968; Mc Bride and Zehr, 1981; Wheeler and Hendon, 2004) than the non-convective phase (Maloy and Hartmann, 2000).

Hence, in order to ascertain the presence of MJO in the study region, we subjected the monthly OLR data from 1979 to 2017 to Morlet wavelet power spectrum analysis. The wavelet analysis clearly showed the presence of three prominent modes that were significant at 95% confidence level (Fig. 9). Most of the energy of the power spectrum was in the annual periodicity followed by semi-annual periodicity, indicated by the horizontal closed contours. The third dominant variability was in the 30-90 day band indicated by the closed vertical elliptical contours and it was prominently seen during the years 1987, 1997, 2007, and 2015. Thus, the wavelet analysis confirms that the intra-seasonal variability which includes MJO was present in 2015. To pinpoint the duration in which the MJO was active we analyzed the hovmoller diagram of 15 to 90 day band passed 5-day running mean of daily OLR (Fig.10 left panel), a proxy for deep convection in tropics (Liebmann and Hartmann, 1982), and zonal wind at 850 hPa (Fig. 10 right panel) averaged over 5°S to 5°N from 44°E to 100°E for the period 15<sup>th</sup> February to 20<sup>th</sup> December 2015. In Fig. 10 (left panel) a negative OLR appears at 50°E on 25<sup>th</sup> October which moves eastward with time reaching 90°E by 15<sup>th</sup> November. A similar eastward propagation is also seen in the zonal wind at 850 hPa with westerly winds propagating towards the east. The eastward propagation of both negative OLR and westerly wind indicated the MJO signal which arrives in the vicinity of 65°-66°E during 28<sup>th</sup> October and persists there until 5<sup>th</sup> November. The location and time of the arrival of the MJO signal coincide with the time and location of the origin of cyclones Chapala and Megh. The computation of correlation of OLR with the depth of 26°C isotherm ( $D_{26}$ ) in the region of origin of Chapala, Box A, from 28<sup>th</sup> October to 4<sup>th</sup> November 2015 showed an inverse relationship with the correlation coefficient of 0.69 and was

significant at 95% confidence level. This indicated that the enhanced convection caused by MJO during Chapala was associated with deep  $D_{26}$ . Thus, the arrival of MJO triggers convection and deep  $D_{26}$  augments its further intensification. Since  $D_{26}$  could be taken as the proxy for the TCHP (see Eq.3), the deep  $D_{26}$  implies that the region had sufficient heat content in the upper ocean to support enhanced convection and its intensification during Chapala. Recall that on 28<sup>th</sup> October the low pressure, which was centered at 11.5°N and 65°E, intensified into a depression. IMD also reported that this region was under the influence of MJO with amplitude greater than 2 (<http://www.rsmcnewdelhi.imd.gov.in/images/pdf/publications/preliminary-report/chap.pdf>).

All of the above showed a favorable condition for cyclogenesis coinciding with the arrival of the MJO signal. A similar result was obtained by Camargo et al. (2009) who reported an increase in the mid-level moisture flux and low-level vorticity during the active phase of MJO in the Indian Ocean during the August-October period. Thus, it would seem that the trigger for the origin of cyclone Chapala on 28<sup>th</sup> October 2015 in the southeastern Arabian Sea was linked to the arrival of atmospheric deep convection and the westerly winds associated with eastward propagating MJO signal. The deep convection weakens the vertical wind shear and increases the mid-level moisture flux, a condition that favours the cyclogenesis.

Though the co-occurrence of strongest El Niño and positive IOD along with the associated processes pre-conditioned the western AS for the cyclogenesis and the arrival of MJO as a trigger could explain the formation of Chapala, the generation of another cyclone in the same region within a week time would need another mechanism. Since the SST threshold for the genesis of a cyclone is in excess of 26°C, we examined the time evolution of the depth of 26°C isotherm ( $D_{26}$ ) along a zonal band 13-15°N in the AS during January 2014 to December 2015 (Fig. 11a). The  $D_{26}$  during the period from the end of October to the first week of November in 2015 was 60 m which was at least 10 m deeper in comparison to the same period in the previous year. Since  $D_{26}$  could be taken as the proxy for the TCHP (see Eq.3), the deep  $D_{26}$  implies that the region where the Chapala and Megh originated would have had sufficient heat content in the upper ocean for generating 2 cyclones back-to-back. This brings us to the question of what caused the deepening of  $D_{26}$  in 2015. To explore this we plotted the time-longitude diagram of sea level anomaly (SLA) (Fig. 11b) for the period from August 2014 to December 2015. The figure reveals the presence of a downwelling Rossby wave, which arrives at the generating area of the cyclone Megh at the end of October. This resulted in a positive SLA of 15-20 cm in 2015. However, in 2014 the signature of the Rossby wave propagation is weaker and SLA was 0-5 cm. The computation of correlation of SLA with  $D_{26}$  in the region of

origin of Megh, Box B, from 5<sup>th</sup> to 10<sup>th</sup> November 2015 showed a linear relationship with the correlation coefficient of 0.85 and was significant at 98% confidence level. In contrast, the correlation of  $D_{26}$  and surface wind speed showed an inverse relationship with a correlation coefficient of 0.84 and was significant at 97% confidence level. This indicated that the deepening of  $D_{26}$  was not associated with the local wind but associated with high SLA associated with Rossby wave propagation during the period of Chapala. Seiki et al. (2015) observed a westward migration of positive SST anomaly concurrently with down-welling annual Rossby waves that occur in the south equatorial Indian Ocean.

Thus, based on the above results we propose that the necessary oceanic condition in terms of high SST and deep  $D_{26}$  in 2015 was created by the stronger downwelling Rossby wave lead to high TCHP, while the MJO triggered the generation of cyclone by lowering the vertical wind shear and increasing the relative vorticity and mid-troposphere relative humidity. We believe that the co-occurrence of the positive phase of IOD and El Niño pre-conditioned the western AS in terms of warm SST, intense atmospheric convection, and increased moisture input through altered Walker Circulation, and set the stage congenial for the formation of a cyclone. The arrival of eastward propagating MJO and associated deep convection provided the necessary trigger for the formation of cyclone Chapala. The stronger than normal westward propagating down-welling Rossby wave provided the necessary thermal energy in terms of increase TCHP to the water column by deepening the thermocline so that the second cyclone Megh could be triggered in the same region within a week of the origin of Chapala. This has been illustrated in a schematic in Fig.12. Note that the unusually warm waters in the western AS were a result of the co-occurrence of strong El Niño and positive IOD in 2015 with colder than normal waters in the eastern Indian Ocean. The resulting reverse-Walker Circulation with surface divergence and deep convection in the western AS and surface divergence associated with the sinking of air mass in the eastern Indian Ocean. The propagation of the MJO signal as well as Rossby waves in the AS is also shown.

## **7. Concluding Remarks**

The back-to-back occurrence of tropical cyclones is an extremely rare phenomenon due to the requirement that several oceans and atmospheric conditions such as SST in excess of 26°C, low-level wind convergence, high relative vorticity, weak vertical wind shear, and high relative humidity must co-occur. The threshold value of SST for initiating the convection and the formation of a tropical cyclone is 26.5°C (Palmen, 1956; Gray, 1968; Tory and Dare, 2015), while the threshold value for the vertical wind shear should be less than 10m/s for the formation of tropical

cyclone (Evan and Camargo, 2011). After the generation of a cyclone, the upper ocean undergoes cooling of at least a couple of degrees and hence it would take several weeks for the same region to heat up to attain an SST in excess of 26°C, which is one of the necessary condition. In the AS the back-to-back occurrence of Chapala and Megh in the same region within a span of 8 days (28<sup>th</sup> October and 5<sup>th</sup> November respectively) is perhaps for the first time. The only other known occurrence was in 1997 when two tropical storms 3 and 4, separated by 12-degree longitude and 3-degree latitude, occurred during 4 to 10<sup>th</sup> and 2 to 14<sup>th</sup> November respectively.

The upper ocean response of cyclones Chapala and Megh was in terms of cooling of SST, which was 1.5°C and 1.0°C respectively. The upper-ocean cooling in parts was due to wind-driven evaporative cooling and wind stress curl- induced upward Ekman pumping of subsurface cold waters to the upper ocean. Argo floats in the vicinity of the cyclone tracks also captured cooling in SST as well as the mixed layer deepening of 37 m due to the cyclone. The upward Ekman pumping, in turn, impacts the chlorophyll biomass and CO<sub>2</sub> flux as the upwelled subsurface cold water is rich in nutrients and CO<sub>2</sub>. Subsequently, Chl-a showed a 6-fold increase from its pre-cyclone value of 0.36 mg/m<sup>3</sup> for Chapala, while Megh showed a 2-fold from its pre-cyclone values of 0.30 mg/m<sup>3</sup>. The bio-Argo float captured the cyclone-induced chlorophyll response in terms of 10-fold increase in surface Chl-a values from its pre-cyclone value of 0.1 mg/m<sup>3</sup>. Consistent with the chlorophyll increase, the NPP also showed an increase of 5.8 times from its pre-cyclone value of 496.26 mg C m<sup>-2</sup> day<sup>-1</sup> for Chapala and 1.5 times from its pre-cyclone value of 518.63 mg C m<sup>-2</sup> day<sup>-1</sup> for Megh. The CO<sub>2</sub> flux showed a 6-fold and 2-fold increase respectively for Chapala and Megh compared to the pre-cyclone value of 2.69-3.58 and 6.78 mmol m<sup>-2</sup> day<sup>-1</sup>.

The exceptional occurrence of Chapala and Megh was facilitated by the anomalous co-occurrence of the positive phase of IOD and El Niño along with the arrival of MJO at the location where both cyclones originated. Both the positive phase of IOD and El Niño supported large scale warming of the upper ocean and associated atmospheric convection in the western Indian Ocean including large parts of the AS and cooling and subsidence in the eastern Equatorial Indian Ocean due to the shifting of the Walker Circulation. This pre-conditioned both ocean and atmosphere creating the situation congenial for the generation of the cyclone and the arrival of eastward propagation MJO finally triggered the cyclogenesis. Though the upper ocean experienced cooling after the generation of first cyclone Chapala, the deep D<sub>26</sub> under the influence of the downwelling Rossby wave had sufficient energy in the upper ocean to support a second cyclone Megh within a week of the first one. We wish to submit that though it was possible to unravel the dynamics and thermodynamics that lead to the back-to-back formation of Chapala and Megh with the help of a suite of remote

sensing data and limited in situ Argo data, it is necessary to examine the above-suggested mechanism with the help of ocean-atmosphere coupled model simulation. In addition to the above climate scale changes such as MJO, ENSO, and IOD, anthropogenic global warming also can influence the tropical cyclone activity. For e.g., Wehner et al. (2018) using high-resolution global climate model simulation showed that even at low warming levels the frequency and intensity of the most intense cyclone showed an increase while the weaker tropical cyclones decreased.

## **Acknowledgments**

The authors thank Directors of Indian Institute of Technology (IIT), Kharagpur and CSIR-National Institute of Oceanography (CSIR-NIO), Goa and the Council of Scientific and Industrial Research (CSIR), New Delhi for all the support and encouragement for this research. Riyanka Roy Chowdhury acknowledges the Ministry of Human Resource Development (MHRD), Government of India for providing the research fellowship. Cyclone track data used in this paper is from IMD best tracks data

([http://www.rsmcnewdelhi.imd.gov.in/index.php?option=com\\_content&view=article&id=48&Itemid=194&lang=en](http://www.rsmcnewdelhi.imd.gov.in/index.php?option=com_content&view=article&id=48&Itemid=194&lang=en)). SST data is available in the APDRC Live Access Server which is freely accessible (<http://apdrc.soest.hawaii.edu/las/v6/constrain?var=1234>). Multi-mission satellite product from Jason-3, sentinel-3A, Cyrosat, Saral/Altika, ENVISAT, GFO, TOPEX/Poseidon combined altimeter products used in this study can be obtained from the website

([http://marine.copernicus.eu/services-portfolio/access-to-products/?option=com\\_csw&view=details&product\\_id=SEALEVEL\\_GLO\\_PHY\\_L4\\_REP\\_OBSERVATIONS\\_008\\_047](http://marine.copernicus.eu/services-portfolio/access-to-products/?option=com_csw&view=details&product_id=SEALEVEL_GLO_PHY_L4_REP_OBSERVATIONS_008_047)).

Surface wind product used for this study was obtained from ASCAT and NECP reanalysis (<http://apdrc.soest.hawaii.edu/las/v6/dataset?catitem=12664>); (<https://www.esrl.noaa.gov/psd/data/gridded/data.ncep.reanalysis.pressure.html>). TCHP and OHC data were taken from the APDRC website (<http://apdrc.soest.hawaii.edu/las/v6/constrain?var=3227>)(<http://apdrc.soest.hawaii.edu/las/v6/constrain?var=3059>) . HYCOM global reanalysis data used in this study were obtained from the website ([http://apdrc.soest.hawaii.edu/las\\_ofes/v6/dataset?catitem=229](http://apdrc.soest.hawaii.edu/las_ofes/v6/dataset?catitem=229)). FNMOC data are taken from the ERDDAP data server (<https://coastwatch.pfeg.noaa.gov/erddap/griddap/erdlasFnPres6.html>). ARGO floats data freely made available by the international and national Argo program were downloaded from the website (<http://www.coriolis.eu.org/Data-Products/Data-Delivery/Data-selection>). NOAA interpolated data used in this study were taken from the website (<https://www.ncei.noaa.gov/data/outgoing-longwave-radiation-daily/access/>). NCEP climate forecast



system data were downloaded from the website (<http://apdrc.soest.hawaii.edu/las/v6/dataset?catitem=3007>). NCEP reanalysis data were obtained from the NOAA ESRL (<https://www.esrl.noaa.gov/psd/data/gridded/data.ncep.html>). NASA Ocean color data pertaining to daily Chl-a was taken from the website ([https://oceandata.sci.gsfc.nasa.gov/MODIS-Aqua/Mapped/Daily/4km/chlor\\_a/](https://oceandata.sci.gsfc.nasa.gov/MODIS-Aqua/Mapped/Daily/4km/chlor_a/)), while the monthly mean Chl-a climatology was taken from the website ([https://oceandata.sci.gsfc.nasa.gov/SeaWiFS/Mapped/Monthly\\_Climatology/9km/chlor\\_a/](https://oceandata.sci.gsfc.nasa.gov/SeaWiFS/Mapped/Monthly_Climatology/9km/chlor_a/)). The NPP data was taken from the website (<https://coastwatch.pfeg.noaa.gov/erddap/griddap/erdMH1pp1day.html>). The information on IOD and El Niño years was obtained from the websites <http://www.bom.gov.au/climate/iod/> and <https://ggweather.com/enso/oni.htm> respectively. The figures are generated using MATLAB and Ferret. The authors thank the three anonymous reviewers for their constructive suggestions that helped to improve the quality of the manuscript. NIO contribution number XXXX.

## References

- Alimohammadi, M., & Malakooti, H. (2018). Sensitivity of simulated cyclone Gonu intensity and track to variety of parameterizations: Advanced hurricane WRF model application. *Journal of Earth System Science*. <https://doi.org/10.1007/s12040-018-0941-4>.
- Balaji, M., Chakraborty, A., & Mandal, M. (2018). Changes in tropical cyclone activity in north Indian Ocean during satellite era (1981–2014). *International Journal of Climatology*. <https://doi.org/10.1002/joc.5463>.
- Banse, K. (1987). Seasonality of phytoplankton chlorophyll in the central and northern Arabian sea. *Deep Sea Research Part A, Oceanographic Research Papers*. [https://doi.org/10.1016/0198-0149\(87\)90032-X](https://doi.org/10.1016/0198-0149(87)90032-X).
- Bates, N. R., Knap, A. H., & Michaels, A. F. (1998). Contribution of hurricanes to local and global estimates of air-sea exchange of CO<sub>2</sub>. *Nature*. <https://doi.org/10.1038/25703>.
- Bauer, S., Hitchcock, G. L., & Olson, D. B. (1991). Influence of monsoonally-forced Ekman dynamics upon surface layer depth and plankton biomass distribution in the Arabian Sea. *Deep Sea Research Part A, Oceanographic Research Papers*. [https://doi.org/10.1016/0198-0149\(91\)90062-K](https://doi.org/10.1016/0198-0149(91)90062-K).
- Behrenfeld, M. J., & Falkowski, P. G. (1997). Photosynthetic rates derived from satellite-based chlorophyll concentration. *Limnology and Oceanography*. <https://doi.org/10.4319/lo.1997.42.1.0001>.
- Brock, J. C., & McClain, C. R. (1992). Interannual variability in phytoplankton blooms observed in the northwestern Arabian Sea during the southwest monsoon. *Journal of Geophysical Research*. <https://doi.org/10.1029/91JC02225>.
- Byju, P., & Prasanna Kumar, S. (2011). Physical and biological response of the Arabian Sea to tropical cyclone Phyan and its implications. *Marine Environmental Research*. <https://doi.org/10.1016/j.marenvres.2011.02.008>.
- Camargo, S. J., Wheeler, M. C., & Sobel, A. H. (2009). Diagnosis of the MJO modulation of tropical cyclogenesis using an empirical index. *Journal of the Atmospheric Sciences*. <https://doi.org/10.1175/2009JAS3101.1>.
- Dube, S. K., Rao, D., Sinha, P. C., Murty, T. S., & Bahuluyan, N. (1997). Storm surge in the Bay of Bengal and Arabian Sea: The problem and its prediction. *Mausam*.48.
- Dube, S. K., Jain, I., Rao, A. D., & Murty, T. S. (2009). Storm surge modelling for the Bay of Bengal and Arabian Sea. In *Natural Hazards*. <https://doi.org/10.1007/s11069-009-9397-9>.
- Emanuel, K. (2005). Increasing destructiveness of tropical cyclones over the past 30 years. *Nature*. <https://doi.org/10.1038/nature03906>
- Evan, A. T., & Camargo, S. J. (2011). A climatology of Arabian Sea cyclonic storms. *Journal of Climate*. <https://doi.org/10.1175/2010JCLI3611.1>.

- Findlater, J. (1969). A major low-level air current near the Indian Ocean during the northern summer. *Quarterly Journal of the Royal Meteorological Society*. <https://doi.org/10.1002/qj.49709540409>.
- Gill, A. E. (1982). Atmosphere - ocean dynamics. *NEW YORK, U.S.A., ACADEMIC PRESS INC., 1982*.
- Goyet, C., Millero, F. J., O'Sullivan, D. W., Eiseheid, G., McCue, S. J., & Bellerby, R. G. J. (1998). Temporal variations of pCO<sub>2</sub> in surface seawater of the Arabian Sea in 1995. *Deep-Sea Research Part I: Oceanographic Research Papers*. [https://doi.org/10.1016/S0967-0637\(97\)00085-X](https://doi.org/10.1016/S0967-0637(97)00085-X).
- Gray, W. M. (1968). Global view of the origin of tropical disturbances and storms. *Monthly Weather Review*. [https://doi.org/10.1175/1520-0493\(1968\)096<0669:gvotoo>2.0.co;2](https://doi.org/10.1175/1520-0493(1968)096<0669:gvotoo>2.0.co;2).
- Grinsted, A., Moore, J. C., & Jevrejeva, S. (2004). Application of the cross wavelet transform and wavelet coherence to geophysical time series. *Nonlinear Processes in Geophysics*. <https://doi.org/10.5194/npg-11-561-2004>.
- Huang, P., Sanford, T. B., & Imberger, J. (2009). Heat and turbulent kinetic energy budgets for surface layer cooling induced by the passage of Hurricane Frances (2004), *J. Geophys. Res.* 114: C12023, doi:10.1029/2009JC005603.
- Huang, B., Thorne, P. W., Banzon, V. F., Boyer, T., Chepurin, G., Lawrimore, J. H., et al. (2017). Extended reconstructed Sea surface temperature, Version 5 (ERSSTv5): Upgrades, validations, and intercomparisons. *Journal of Climate*. <https://doi.org/10.1175/JCLI-D-16-0836.1>.
- Jacob, S. D., Shay, L. K., Mariano, A. J., & Black, P. G. (2000). The 3D oceanic mixed layer response to Hurricane Gilbert, *J. Phys. Oceanogr.* 30: 1407–1429. doi:10.1175/1520-0485(2000)030<1407:TOMLRT>2.0.CO;2.
- Steven, V. H., Denis, P., James, R., Ernie, L., & Wallace, D.W.R.. (2011). CO2SYS v 1.1, MATLAB program developed for CO<sub>2</sub> system calculations. ORNL/CDIAC-105b. Carbon Dioxide Information Analysis Center, Oak Ridge National Laboratory, U.S. DoE, Oak Ridge, TN.
- Kalnay, E., Kanamitsu, M., Kistler, R., Collins, W., Deaven, D., Gandin, L., et al. (1996). The NCEP/NCAR 40-year reanalysis project. *Bulletin of the American Meteorological Society*. [https://doi.org/10.1175/1520-0477\(1996\)077<0437:TNYRP>2.0.CO;2](https://doi.org/10.1175/1520-0477(1996)077<0437:TNYRP>2.0.CO;2).
- Liebmann, B., & Smith, C.A. (1996) Description of a Complete (Interpolated) Outgoing Longwave Radiation Dataset. *Bulletin of the American Meteorological Society*. 77: 1275-1277.
- Madden, R. A., & Julian, P. R. (1971). Detection of a 40–50 Day Oscillation in the Zonal Wind in the Tropical Pacific. *Journal of the Atmospheric Sciences*. [https://doi.org/10.1175/1520-0469\(1971\)028<0702:doadoi>2.0.co;2](https://doi.org/10.1175/1520-0469(1971)028<0702:doadoi>2.0.co;2).
- Madden, R. A., & Julian, P. R. (1972). Description of Global-Scale Circulation Cells in the Tropics with a 40–50 Day Period. *Journal of the Atmospheric Sciences*. [https://doi.org/10.1175/1520-0469\(1972\)029<1109:dogsc>2.0.co;2](https://doi.org/10.1175/1520-0469(1972)029<1109:dogsc>2.0.co;2).

- Madhupratap, M., Prasanna Kumar, S., Bhattathiri, P. M. A., Dileep Kumar, M., Raghukumar, S., Nair, K. K. C., & Ramaiah, N. (1996). Mechanism of the biological response to winter cooling in the northeastern Arabian Sea. *Nature*. <https://doi.org/10.1038/384549a0>.
- Maloney, E. D., & Hartmann, D. L. (2000). Modulation of eastern north Pacific Hurricanes by the Madden-Julian oscillation. *Journal of Climate*. [https://doi.org/10.1175/1520-0442\(2000\)013<1451:MOENPH>2.0.CO;2](https://doi.org/10.1175/1520-0442(2000)013<1451:MOENPH>2.0.CO;2).
- Mandal, M., Mohanty, U. C., & Raman, S. (2004). A study on the impact of parameterization of physical processes on prediction of tropical cyclones over the Bay of Bengal with NCAR/PSU mesoscale model. *Natural Hazards*. <https://doi.org/10.1023/B:NHAZ.0000023359.24526.24>.
- McBride, J. L. (1981). Observational analysis of tropical cyclone formation. Part I: basic description of data sets. *Journal of the Atmospheric Sciences*. [https://doi.org/10.1175/1520-0469\(1981\)038<1117:OAOTCF>2.0.CO;2](https://doi.org/10.1175/1520-0469(1981)038<1117:OAOTCF>2.0.CO;2).
- Mohanty, U. C., & Gupta, A. (2008). Deterministic methods for prediction of tropical cyclone tracks. In *Modelling and Monitoring of Coastal Marine Processes*. [https://doi.org/10.1007/978-1-4020-8327-3\\_10](https://doi.org/10.1007/978-1-4020-8327-3_10).
- Monterey, G., and S. Levitus (1997). Seasonal Variability of Mixed Layer Depth for the World Ocean, *NOAA Atlas NESDIS 14*, U.S. Gov. Print. Off., Washington, D. C.
- Morrison, J. M., Codispoti, L. A., Gaurin, S., Jones, B., Manghnani, V., & Zheng, Z. (1998). Seasonal Variations of Hydrographic and Nutrient Fields during the USJGOFS Arabian Sea Process Study. *Deep Sea Research Part-II: Tropical Studies in Oceanography*. 45: 2053-2101.
- Muni Krishna, K. (2016). Observational study of upper ocean cooling due to Phet super cyclone in the Arabian Sea. *Advances in Space Research*. <https://doi.org/10.1016/j.asr.2016.02.024>.
- Murty, V. S. N., Rao, D.P, & Sastry, J. S., (1983) The lowering of sea surface temperature in the east central Arabian Sea associated with a cyclone. *Mahasagar*.16: 67– 71.
- Naik, H., Naqvi, S. W. A., Suresh, T., & Narvekar, P. V. (2008). Impact of a tropical cyclone on biogeochemistry of the central Arabian Sea. *Global Biogeochemical Cycles*. <https://doi.org/10.1029/2007GB003028>.
- Naqvi, S. W. A., Noronha, R. J., Somasundar, K., & Sen Gupta, R. (1990). Seasonal changes in the denitrification regime of the Arabian Sea. *Deep Sea Research Part A, Oceanographic Research Papers*. [https://doi.org/10.1016/0198-0149\(90\)90092-A](https://doi.org/10.1016/0198-0149(90)90092-A).
- Nemoto, K., Midorikawa, T., Wada, A., Ogawa, K., Takatani, S., Kimoto, H., et al. (2009). Continuous observations of atmospheric and oceanic CO<sub>2</sub> using a moored buoy in the East China Sea: Variations during the passage of typhoons. *Deep-Sea Research Part II: Topical Studies in Oceanography*. <https://doi.org/10.1016/j.dsr2.2008.12.015>.
- Olson, D. B., Hitchcock, G. L., Fine, R. A., & Warren, B. A. (1993). Maintenance of the low-oxygen layer in the central Arabian Sea. *Deep-Sea Research Part II*. [https://doi.org/10.1016/0967-0645\(93\)90051-N](https://doi.org/10.1016/0967-0645(93)90051-N).

- Osuri, K. K., Mohanty, U. C., Routray, A., & Mohapatra, M. (2012). The impact of satellite-derived wind data assimilation on track, intensity and structure of tropical cyclones over the North Indian Ocean. *International Journal of Remote Sensing*. <https://doi.org/10.1080/01431161.2011.596849>.
- Piontkovski, S., & Al-Azri, A. (2010). Influence of a tropical cyclone Gonu on phytoplankton biomass (chlorophyll a) in the Arabian Sea. In *Indian Ocean Tropical Cyclones and Climate Change*. [https://doi.org/10.1007/978-90-481-3109-9\\_38](https://doi.org/10.1007/978-90-481-3109-9_38).
- Plmen, E. H. (1956). A review of knowledge on the formation and development of tropical cyclones, *Proc. Tropical Cyclone Symp.*, Brisbane, QLD, Australia, Bureau of Meteorology, 213-231, 3, 26-38.
- Pollard, R., Rhines, P., & Thompson, R. (1973). The deepening of the wind-mixed layer, *Geophys. Fluid Dyn.* 3: 381–404.
- Prasanna Kumar, S., & Prasad, T. G. (1996). Winter cooling in the northern Arabian Sea. *Current Science*. 71: 834-841.
- Prasanna Kumar, S., Madhupratap, M., Dileep Kumar, M., Muraleedharan, P. M., De Souza, S. N., Gauns, M., & Sarma, V. V. S. S. (2001a). High biological productivity in the central Arabian Sea during the summer monsoon driven by Ekman pumping and lateral advection. *Current Science*. 81: 1633-1638.
- Prasanna Kumar, S., Ramaiah, N., Gauns, M., Sarma, V. V. S. S., Muraleedharan, P. M., Raghukumar, S., et al. (2001b). Physical forcing of biological productivity in the Northern Arabian Sea during the Northeast Monsoon. *Deep-Sea Research Part II: Topical Studies in Oceanography*. [https://doi.org/10.1016/S0967-0645\(00\)00133-8](https://doi.org/10.1016/S0967-0645(00)00133-8).
- Prasanna Kumar, S., Roshin, R. P., Narvekar, J., Kumar, P. K. D., & Vivekanandan, E. (2009). Response of the Arabian Sea to global warming and associated regional climate shift. *Marine Environmental Research*. <https://doi.org/10.1016/j.marenvres.2009.06.010>.
- Price, J. F. (1981). Upper ocean response to a hurricane. *Journal of Physical Oceanography*. [https://doi.org/10.1175/1520-0485\(1981\)011%3C0153:UORTAH%3E2.0.CO;2](https://doi.org/10.1175/1520-0485(1981)011%3C0153:UORTAH%3E2.0.CO;2).
- Reynolds, R. W., Smith, T. M., Liu, C., Chelton, D. B., Casey, K. S., & Schlax, M. G. (2007). Daily high-resolution-blended analyses for sea surface temperature. *Journal of Climate*. <https://doi.org/10.1175/2007JCLI1824.1>.
- Rodenbeck, C., Keeling, R. F., Bakker, D.C.E., Metzl, N., Oslon, A., Sabine, C., & Heimann, M. (2013). Global surface-ocean  $P^{CO_2}$  and sea-air  $CO_2$  flux variability from an observation driven ocean mixed layer scheme. *Ocean Sci.*, 9, 193-216.
- Roxy, M. K., Ritika, K., Terray, P., & Masson, S. (2014). The curious case of Indian Ocean warming. *Journal of Climate*. <https://doi.org/10.1175/JCLI-D-14-00471.1>.
- Roxy, M. K., Ritika, K., Terray, P., Murtugudde, R., Ashok, K., & Goswami, B. N. (2015). Drying of Indian subcontinent by rapid Indian ocean warming and a weakening land-sea thermal gradient. *Nature Communications*. <https://doi.org/10.1038/ncomms8423>.

- Ryther, J. H., Hall, J. R., Pease, A. K., Bakun, A., & Jones, M. M. (1966). Primary organic production in relation to the chemistry and hydrography of the western Indian Ocean. *Limnology and Oceanography*. <https://doi.org/10.4319/lo.1966.11.3.0371>.
- Sabine, C. L., Wanninkhof, R., Key, R. M., Goyet, C., & Millero, F. J. (2000). Seasonal CO<sub>2</sub> fluxes in the tropical and subtropical Indian Ocean. *Marine Chemistry*. [https://doi.org/10.1016/S0304-4203\(00\)00064-5](https://doi.org/10.1016/S0304-4203(00)00064-5).
- Saha, S., Moorthi, S., Wu, X., Wang, J., Nadiga, S., Tripp, P., et al. (2014). The NCEP climate forecast system version 2. *Journal of Climate*. <https://doi.org/10.1175/JCLI-D-12-00823.1>.
- Saji, N. H., Goswami, B. N., Vinayachandran, P. N., & Yamagata, T. (1999). A dipole mode in the tropical Indian ocean. *Nature*. <https://doi.org/10.1038/43854>.
- Sanford, B., et al. (1987). Ocean response to a hurricane. Part I: Observations, *J. Phys. Oceanogr.* 17: 2065–2083. doi:10.1175/1520-0485(1987)017<2065:ORTAHP>2.0.CO;2.
- Sarker, M. A. (2017). Cyclone hazards in the Arabian sea—A numerical modelling case study of Cyclone Nilofar. *Water and Environment Journal*. <https://doi.org/10.1111/wej.12214>.
- Sarma, V. V. S. S., Dileep Kumar, M., & George, M. D. (1998). The central and eastern Arabian Sea as a perennial source of atmospheric carbon dioxide. *Tellus, Series B: Chemical and Physical Meteorology*. <https://doi.org/10.3402/tellusb.v50i2.16095>.
- Sarma, V. V. S. S., Swathi, P. S., Kumar, M. D., Prasanna Kumar, S., Bhattathiri, P. M. A., Madhupratap, M., et al. (2003). Carbon budget in the eastern and central Arabian Sea: An Indian JGOFS synthesis. *Global Biogeochemical Cycles*. <https://doi.org/10.1029/2002gb001978>.
- Seiki, A., Nagura, M., Hasegawa, T & Yoneyama, K. (2015). Seasonal onset of the Madden-Julian oscillation and its relation to Southeastern Indian ocean cooling: *Journal of Meteorological society of Japan*, 93A, 139-156.
- Sharma, G. (1978). Upwelling Off the Southwest Coast of India. *Indian Journal of Geo-Marine Sciences (IJMS)*. 7, 209-218.
- Shay, L. K., Black, P., Mariano, A., Hawkins, J., & Elsberry, R. (1992). Upper ocean response to Hurricane Gilbert, *J. Geophys. Res.* 97(20): 227–248.
- Smith, R. L., & Bottero, J.S (1977). On upwelling in the Arabian Sea. In: Angel M (ed) *A Voyage of Discovery*. Pergamon, New York, 291–304.
- Smith, S. L., & Codispoti, L. A. (1980). Southwest Monsoon of 1979: Chemical and Biological Response of Somali Coastal Waters. *Science*. <https://doi.org/10.1126/science.209.4456.597>.
- Subrahmanyam, B., Rao, K. H., Srinivasa Rao, N., Murty, V. S. N., & Sharp, R. J. (2002). Influence of a tropical cyclone on Chlorophyll-a Concentration in the Arabian Sea. *Geophysical Research Letters*. <https://doi.org/10.1029/2002gl015892>.



- Takahashi, T., Sutherland, S. C., Wanninkhof, R., Sweeney, C., Feely, R. A., Chipman, D. W., et al. (2009). Climatological mean and decadal change in surface ocean pCO<sub>2</sub>, and net sea-air CO<sub>2</sub> flux over the global oceans. *Deep-Sea Research Part II: Topical Studies in Oceanography*. <https://doi.org/10.1016/j.dsr2.2008.12.009>.
- Torrence, C., & Webster, P. J. (1999). Interdecadal changes in the ENSO-monsoon system. *Journal of Climate*, 12: 2679-2690.
- Torrence, C., & Compo, G. P. (1998). A Practical Guide to Wavelet Analysis. *Bulletin of the American Meteorological Society*. [https://doi.org/10.1175/1520-0477\(1998\)079<0061:APGTWA>2.0.CO;2](https://doi.org/10.1175/1520-0477(1998)079<0061:APGTWA>2.0.CO;2).
- Tory, K. J. & Dare, R.A. (2015). Sea surface temperature thresholds for tropical cyclone formation, *Journal of Climate*, 28, 8171-8183.
- Trenberth, K. (2005). Uncertainty in hurricanes and global warming. *Science*. <https://doi.org/10.1126/science.1112551>.
- Wanninkhof, R. (2014). Relationship between wind speed and gas exchange over the ocean revisited. *Limnology and Oceanography: Methods*. <https://doi.org/10.4319/lom.2014.12.351>.
- Webster, P. J. (2006). Response to Comment on "Changes in Tropical Cyclone Number, Duration, and Intensity in a Warming Environment". *Science*. <https://doi.org/10.1126/science.1121564>.
- Wehner, M. F., Reed, K. A., Loring, B., Stone, D., & Krishnan, H. (2018). Changes in tropical cyclones under stabilized 1.5 and 2.0°C global warming scenarios as simulated by the Community Atmospheric Model under the HAPPI protocols. *Earth Syst. Dynam.*, 9, 187-195, 2018.
- Weiss, R. F. (1974). Carbon dioxide in water and seawater: the solubility of a non-ideal gas. *Marine Chemistry*. [https://doi.org/10.1016/0304-4203\(74\)90015-2](https://doi.org/10.1016/0304-4203(74)90015-2).
- Wheeler, M. C., & Hendon, H. H. (2004). An all-season real-time multivariate MJO index: Development of an index for monitoring and prediction. *Monthly Weather Review*. [https://doi.org/10.1175/1520-0493\(2004\)132<1917:AARMMI>2.0.CO;2](https://doi.org/10.1175/1520-0493(2004)132<1917:AARMMI>2.0.CO;2).
- Yu, J., & Wang, Y. (2009). Response of tropical cyclone potential intensity over the north Indian Ocean to global warming. *Geophysical Research Letters*. <https://doi.org/10.1029/2008GL036742>.
- Zhang, C. (2005). Madden-Julian Oscillation. *Reviews of Geophysics*. <https://doi.org/10.1029/2004RG000158>.



## Figure Captions

**Figure 1** Map showing the annual mean climatology (1997-2010) of chlorophyll-a pigment concentration ( $\text{mg}/\text{m}^3$ ) from SeaWiFS (colour shading) overlaid with seasonal mean climatology (1948-2016) of winds ( $\text{m}/\text{s}$ ) at 10 m from NECP reanalysis for the months of June-July-August. The rectangle in the broken red line is the area of winter bloom (November-February), while the ellipses in the broken red line are the regions where summer-bloom (June-September) occurs. The broad arrow in blue indicates the Findlater Jet that becomes active during the summer monsoon. The solid line in white represents the region of OMZ, while the broken line in white represents the 200 m depth contour. See the text for details.

**Figure 2** Map showing the tracks of the tropical cyclone (red filled diamonds joined by the black solid line) (a) Chapala from 28<sup>th</sup> October to 4<sup>th</sup> November 2015 and (b) Megh from 5<sup>th</sup> to 10<sup>th</sup> November 2015 in the Arabian Sea obtained from IMD. The shading is (a) the difference between SST averaged for 28<sup>th</sup> October to 4<sup>th</sup> November 2015 and SST ( $^{\circ}\text{C}$ ) October-November climatology, and (b) the difference between SST averaged for 5<sup>th</sup> to 10<sup>th</sup> November 2015 and SST ( $^{\circ}\text{C}$ ) October-November climatology. Blue patches are the waters colder than the October-November climatology compared to the cyclone periods. The expansions of abbreviations are D-depression, DD-deep depression, CS-cyclonic storm, SCS-severe cyclonic storm, VSCS-very severe cyclonic storm, and ESCS-extremely severe cyclonic storm. Green filled circles are the locations of Bio-Argo float with ID-2902120 during the cyclone period. Locations of Box A and Box B are also shown on the map. See text for details

**Figure 3** Time evolution of (a) SST ( $^{\circ}\text{C}$ ), tropical cyclone heat potential (TCHP,  $\text{KJ}/\text{m}^2$ ), Ekman pumping velocity (EKV,  $\text{m}/\text{day}$ ) and (b) carbon dioxide flux ( $\text{mmol m}^{-2} \text{day}^{-1}$ ) along the track of cyclone Chapala (solid lines) and Megh (broken lines) from 24<sup>th</sup> October to 14<sup>th</sup> November. Shading from 28<sup>th</sup> October to 4<sup>th</sup> November and from 5<sup>th</sup> November to 10<sup>th</sup> November represents the period of cyclone Chapala and Megh respectively. Markers on the x-axis, both top, and bottom, represent the changes in the intensity of the cyclones. The red and blue dots in the map located in the topmost right corner are the tracks of cyclone Chapala and Megh respectively.

**Figure 4** Time evolution of 3-day composite of chlorophyll *a* pigment concentration (Chl-*a*,  $\text{mg}/\text{m}^3$ ) and pixel count (%) along the track of cyclone (a) Chapala from 21 October to 14 November 2015 and (b) Megh from 21 October to 14 November 2015, and (c) net primary production (NPP,  $\text{mg C m}^{-2} \text{day}^{-1}$ ) for Chapala and Megh. Shading represents the period 28<sup>th</sup> October to 4<sup>th</sup> November 2015 covering the life cycle of the cyclone Chapala and the period 5<sup>th</sup> to 10<sup>th</sup> November 2015 covering the life cycle of the cyclone Megh. Markers show the changes in the intensity of the cyclones.

**Figure 5** Time series of vertical profiles of (a) temperature ( $^{\circ}\text{C}$ ), (b) salinity (psu), (c) chlorophyll *a* ( $\text{mg}/\text{m}^3$ ) and (d) dissolved oxygen (micromole/kg) obtained from Argo float ID 2902120 located near the origin of both Chapala and Megh. The solid horizontal line shows the isothermal layer (ILD) depth and the broken horizontal line represent the mixed layer depth (MLD).

**Figure 6:** Spatial differences between October-November climatology (2010-2016) and October-November 2015 of (a) SST ( $^{\circ}\text{C}$ ), (b) oceanic heat content (OHC,  $\text{KJ}/\text{m}^2$ ), (c) tropical cyclone heat potential (TCHP,  $\text{KJ}/\text{m}^2$ ), (d) relative vorticity at 850 hPa ( $\text{s}^{-1}$ ), (e) vertical wind shear between 850 and 200 hPa ( $\text{m}/\text{s}$ ), and (f) relative humidity at 500 hPa (%) in the Arabian Sea.

**Figure 7** Spatial distribution of (a,b) vertical wind shear between 200 and 850 hPa (m/s), (c, d) lower-tropospheric relative vorticity (850 hPa;  $s^{-1}$ ), and (e, f) mid-tropospheric relative humidity (500 hPa; %). The left panels (a, c, e) are for 27<sup>th</sup> October 2015 and right panels (b, d, f) are for 4<sup>th</sup> November 2015. The magenta filled asterisk and circle denote the location of origin of Chapala in left panels and Megh in the right panel respectively.

**Figure 8** Spatial distribution of SST anomaly and SST climatology (left panels) and sea level pressure (SLP) anomaly and SLP climatology (right panels) composited for (a, d) the cyclone period from 28<sup>th</sup> October to 10<sup>th</sup> November 2015, (b, e) composited for October-November 2015 (c, f) and October-November climatology. The white broken lines in (a), (b), (d) & (e) indicate the zero contours. The vectors overlaid in (d) & (e) are the sea surface wind anomaly, while that in (f) is the surface wind climatology. The filled blue and red diamonds are the locations of the origin of cyclones Chapala and Megh respectively.

**Figure 9** Morlet wavelet power spectrum of monthly mean outgoing longwave radiation (OLR) for the period 1979-2017. The black broken line enclosing the conical region in the figure depicts the area where the signal is 95% significance.

**Figure 10** Five-day running mean of (left panel) outgoing longwave radiation (OLR,  $w/m^2$ ) and (right panel) zonal wind (m/s) at 850 hPa averaged over 5°S to 5°N from 44°E to 100°E for the period 1<sup>st</sup> May to 31<sup>st</sup> December 2015. The horizontal black broken line indicates the period of the cyclones Chapala and Megh, while the slanting broken white line indicates the propagation of negative OLR (intense convection) and negative zonal wind (westerly winds).

**Figure 11** Monthly variation of (a) depth of 26°C isotherm (m) and (b) sea level anomaly (SLA, m) along 13-15°N from 48°E to 72°E in the Arabian Sea from January 2014 to December 2015.

**Figure 12** Schematic diagram showing the process that led to the generation of back-to-back cyclones Chapala and Megh in the Arabian Sea during October-November 2015. See the text for details.

## Appendix A: List of Acronyms

APDRC	Asia-Pacific Data Research Centre
AS	Arabian Sea
ASCAT	Advanced Scatterometer
CFSR	Climate Forecast System Reanalysis
Chl-a	Chlorophyll-a
CMEMS	Copernicus Marine Environment Monitoring Services
CS	Cyclonic Storm
D	Depression
D26	Depth of 26° Isotherm
DD	Deep Depression
DMI	Dipole Mode Index
EKV	Ekman Pumping Velocity
ENSO	El Niño Southern Oscillation
ERSST	Extended Reconstructed SST
ESCS	Extremely Severe Cyclonic Storm
HYCOM	Hybrid Coordinate Ocean Model
ILD	Isothermal Layer Depth
IMD	Indian Meteorological Department
IOD	Indian Ocean Dipole
JGOFS	Joint Global Ocean Flux Studies
MJO	Madden Julian Oscillation
MLD	Mixed Layer Depth
MODIS	Moderate Resolution Imaging Spectro-radiometer
NASA	National Aeronautics and Space Administration
NCEP	National Centre for Environmental Prediction
NIO	North Indian Ocean
NOAA	National Oceanic and Atmospheric Administration
NPP	Net Primary Productivity
OHC	Oceanic Heat Content
OISST	Optimum Interpolation SST
OLR	Outgoing Longwave Radiation
OMZ	Oxygen Minimum Zone
RH	Relative Humidity
SCS	Severe Cyclonic Storm
SLA	Sea Level Anomaly

SLP	Sea Level Pressure
SST	Sea Surface Temperature
TCHP	Tropical Cyclone Heat Potential
VGPM	Vertically Generalized Productivity Model
VSCS	Very Severe Cyclonic Storm

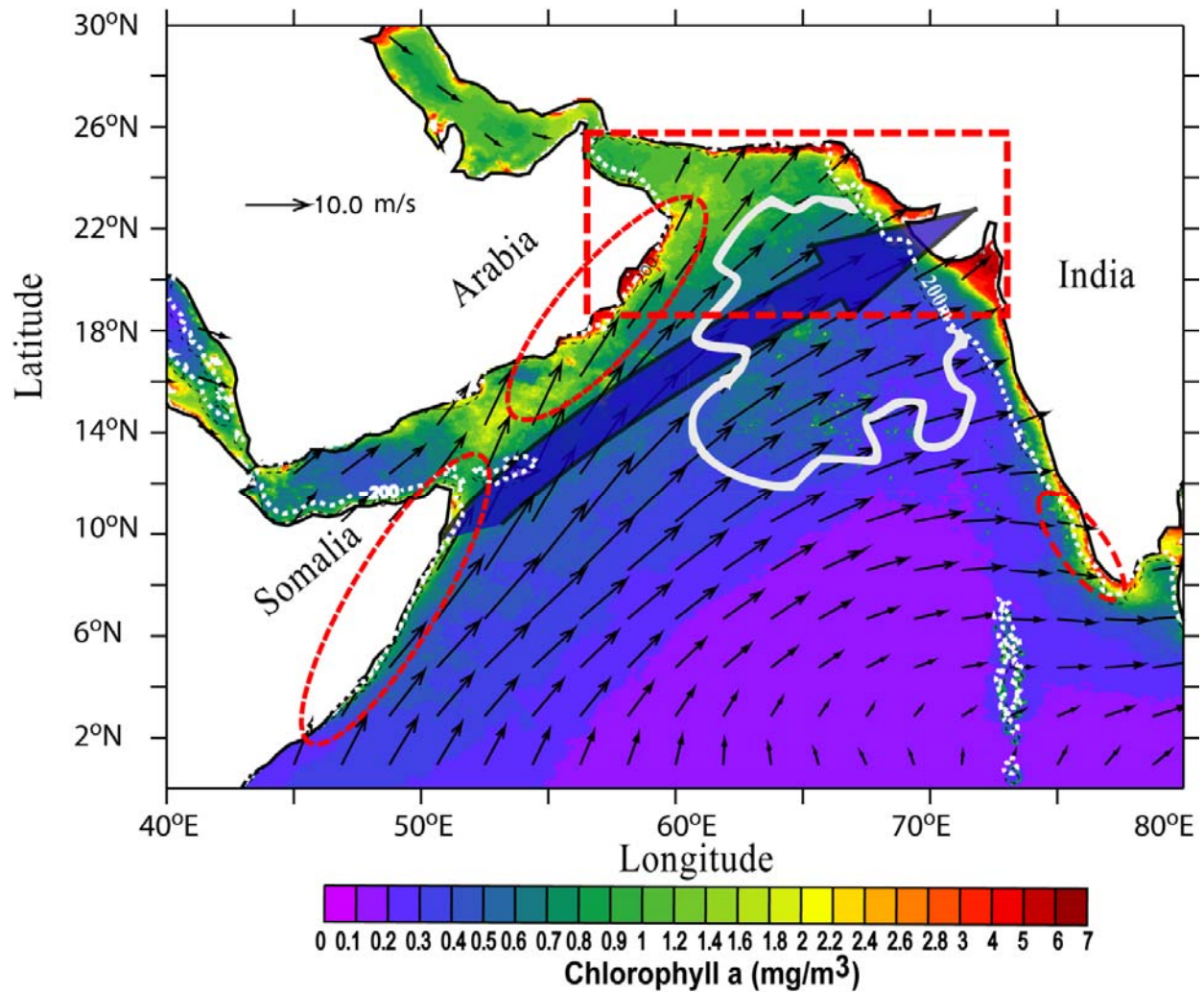


**Figure 1** Map showing the annual mean climatology (1997-2010) of chlorophyll-a pigment concentration (mg/m<sup>3</sup>) from SeaWiFS (colour shading) overlaid with seasonal mean climatology (1948-2016) of winds (m/s) at 10 m from NECP reanalysis for the months of June-July-August. The rectangle in the broken red line is the area of winter bloom (November-February), while the ellipses in the broken red line are the regions where summer-bloom (June-September) occurs. The broad arrow in blue indicates the Findlater Jet that becomes active during the summer monsoon. The solid line in white represents the region of OMZ, while the broken line in white represents the 200 m depth contour. See the text for details.

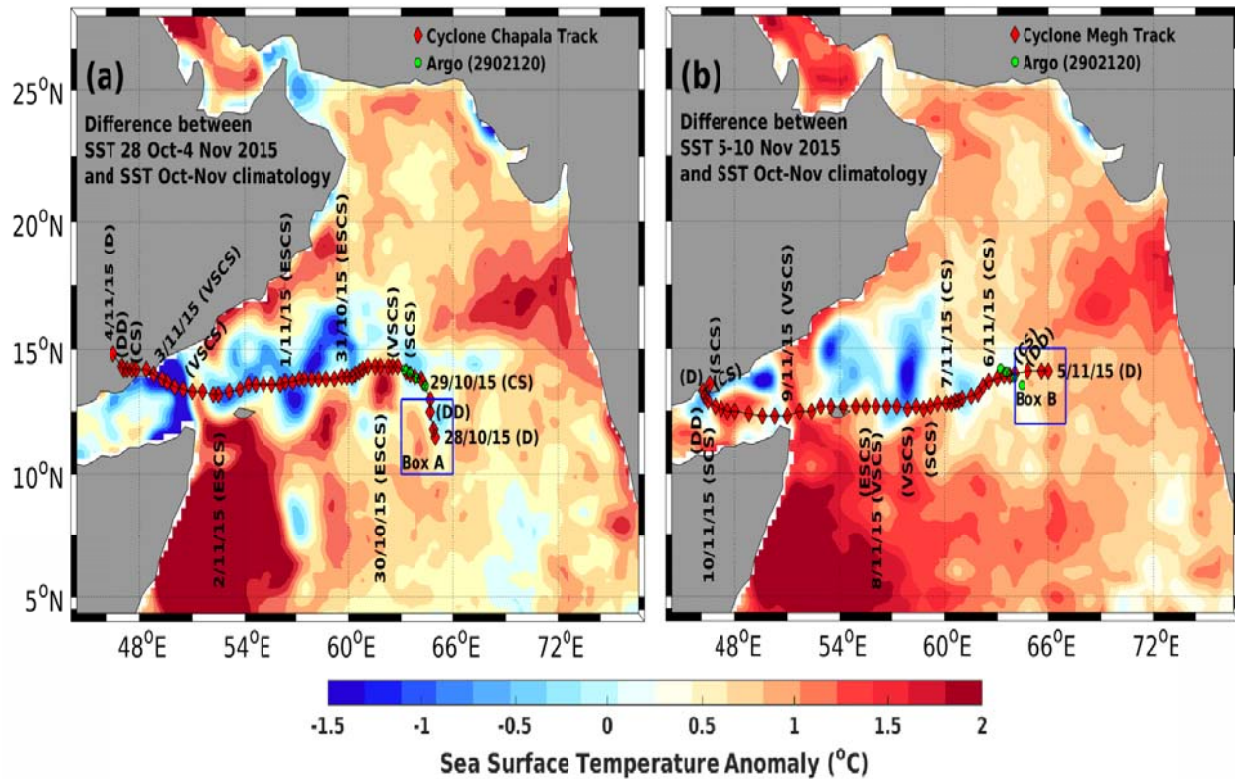


**Figure 2** Map showing the tracks of the tropical cyclone (red filled diamonds joined by the black solid line) (a) Chapala from 28th October to 4th November 2015 and (b) Megh from 5th to 10th November 2015 in the Arabian Sea obtained from IMD. The shading is (a) the difference between SST averaged for 28th October to 4th November 2015 and SST (oC) October-November climatology, and (b) the difference between SST averaged for 5th to 10th November 2015 and SST (oC) October-November climatology. Blue patches are the waters colder than the October-November climatology compared to the cyclone periods. The expansions of abbreviations are D-depression, DD-deep depression, CS-cyclonic storm, SCS-severe cyclonic storm, VSCS-very severe cyclonic storm, and ESCS-extremely severe cyclonic storm. Green filled circles are the locations of Bio-Argo float with ID-2902120 during the cyclone period. Locations of Box A and Box B are also shown on the map. See text for details.



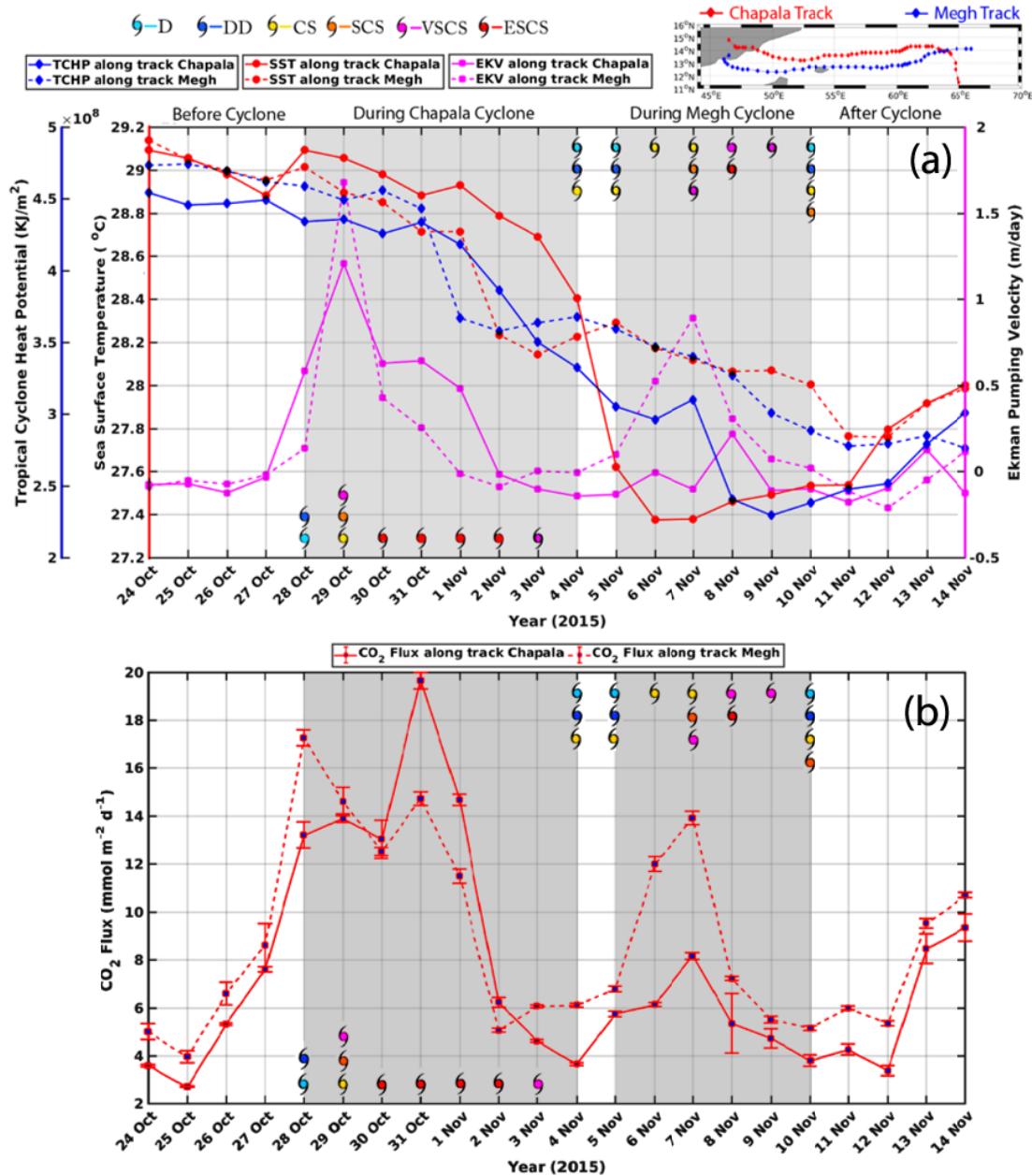


**Figure 3** Time evolution of (a) SST ( $^{\circ}\text{C}$ ), tropical cyclone heat potential (TCHP,  $\text{KJ/m}^2$ ), Ekman pumping velocity (EKV,  $\text{m/day}$ ) and (b) carbon dioxide flux ( $\text{mmol m}^{-2} \text{day}^{-1}$ ) along the track of cyclone Chapala (solid lines) and Megh (broken lines) from 24<sup>th</sup> October to 14<sup>th</sup> November. Shading from 28<sup>th</sup> October to 4<sup>th</sup> November and from 5<sup>th</sup> November to 10<sup>th</sup> November represents the period of cyclone Chapala and Megh respectively. Markers on the x-axis, both top, and bottom, represent the changes in the intensity of the cyclones. The red and blue dots in the map located in the topmost right corner are the tracks of cyclone Chapala and Megh respectively.



**Figure 4** Time evolution of 3-day composite of chlorophyll *a* pigment concentration (Chl-*a*, mg/m<sup>3</sup>) and pixel count (%) along the track of cyclone (a) Chapala from 21 October to 14 November 2015 and (b) Megh from 21 October to 14 November 2015, and (c) net primary production (NPP, mg C m<sup>-2</sup> day<sup>-1</sup>) for Chapala and Megh. Shading represents the period 28<sup>th</sup> October to 4<sup>th</sup> November 2015 covering the life cycle of the cyclone Chapala and the period 5<sup>th</sup> to 10<sup>th</sup> November 2015 covering the life cycle of the cyclone Megh. Markers show the changes in the intensity of the cyclones.

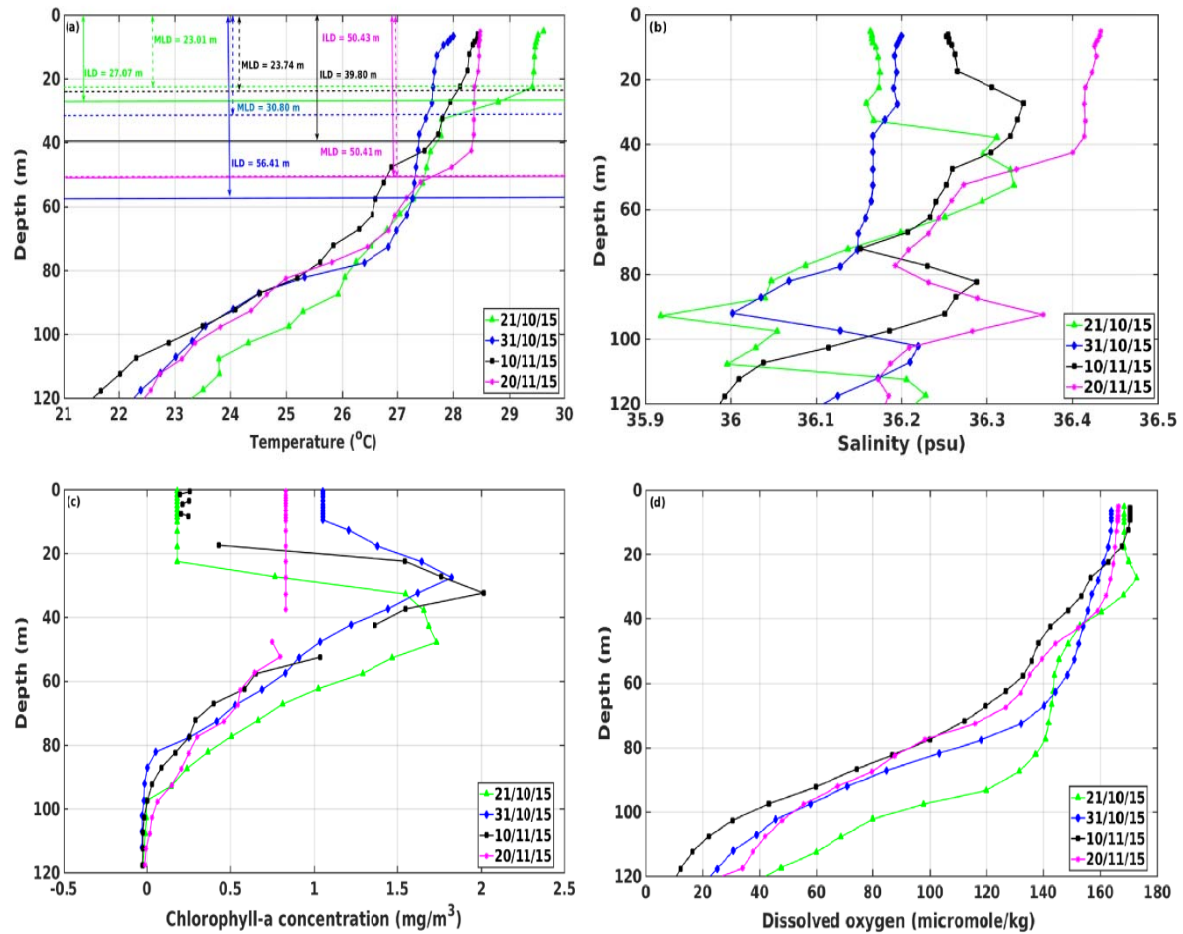


**Figure 5:** Time series of vertical profiles of (a) temperature ( $^{\circ}\text{C}$ ), (b) salinity (psu), (c) chlorophyll *a* ( $\text{mg}/\text{m}^3$ ) and (d) dissolved oxygen (micromole/kg) obtained from Argo float ID 2902120 located near the origin of both Chapala and Megh. The solid horizontal line shows the isothermal layer (ILD) depth and the broken horizontal line represent the mixed layer depth (MLD).

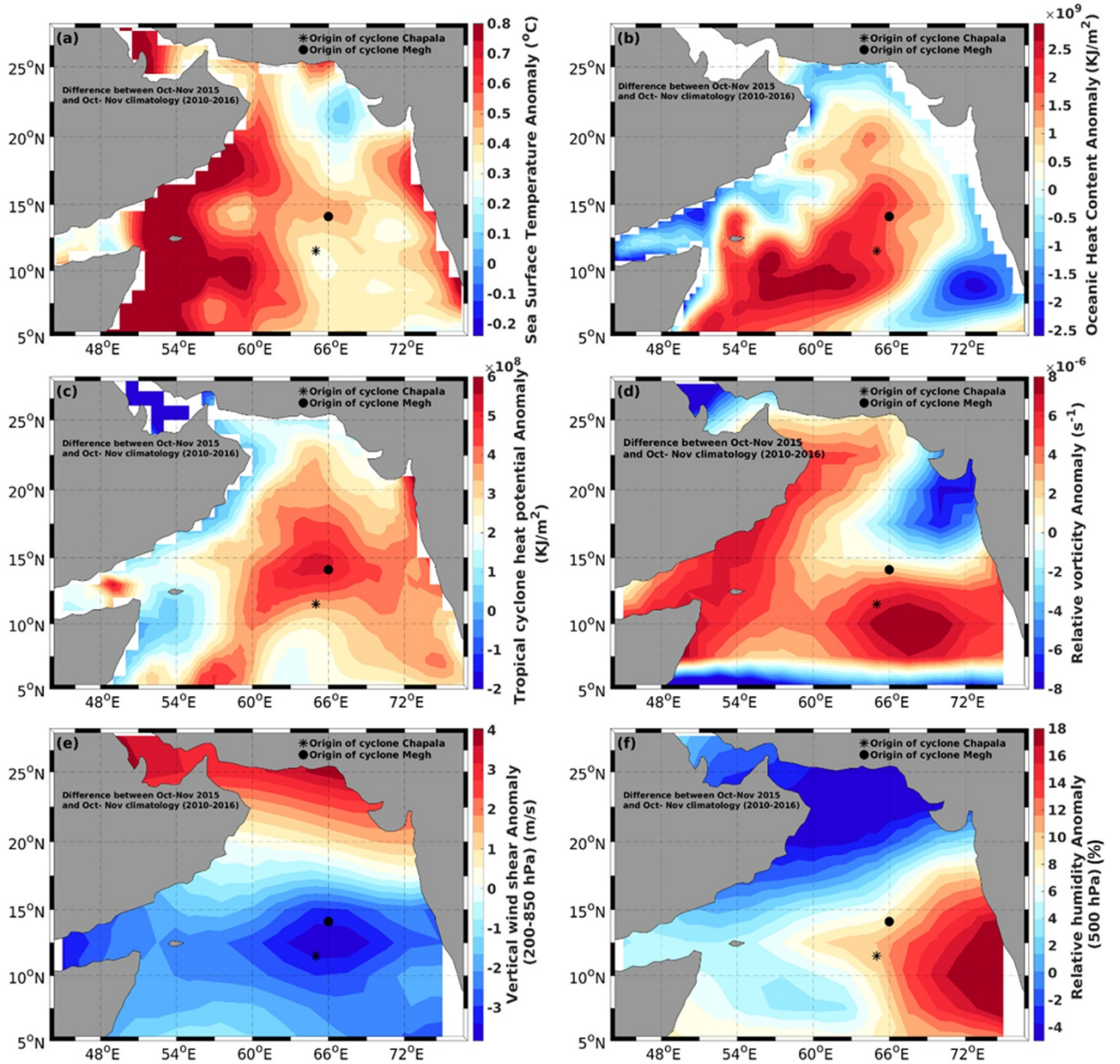


**Figure 6** Spatial differences between October-November climatology (2010-2016) and October- November 2015 of (a) SST (°C), (b) oceanic heat content (OHC, KJ/m<sup>2</sup>), (c) tropical cyclone heat potential (TCHP, KJ/m<sup>2</sup>), (d) relative vorticity at 850 hPa (s<sup>-1</sup>), (e) vertical wind shear between 850 and 200 hPa (m/s), and (f) relative humidity at 500 hPa (%) in the Arabian Sea.

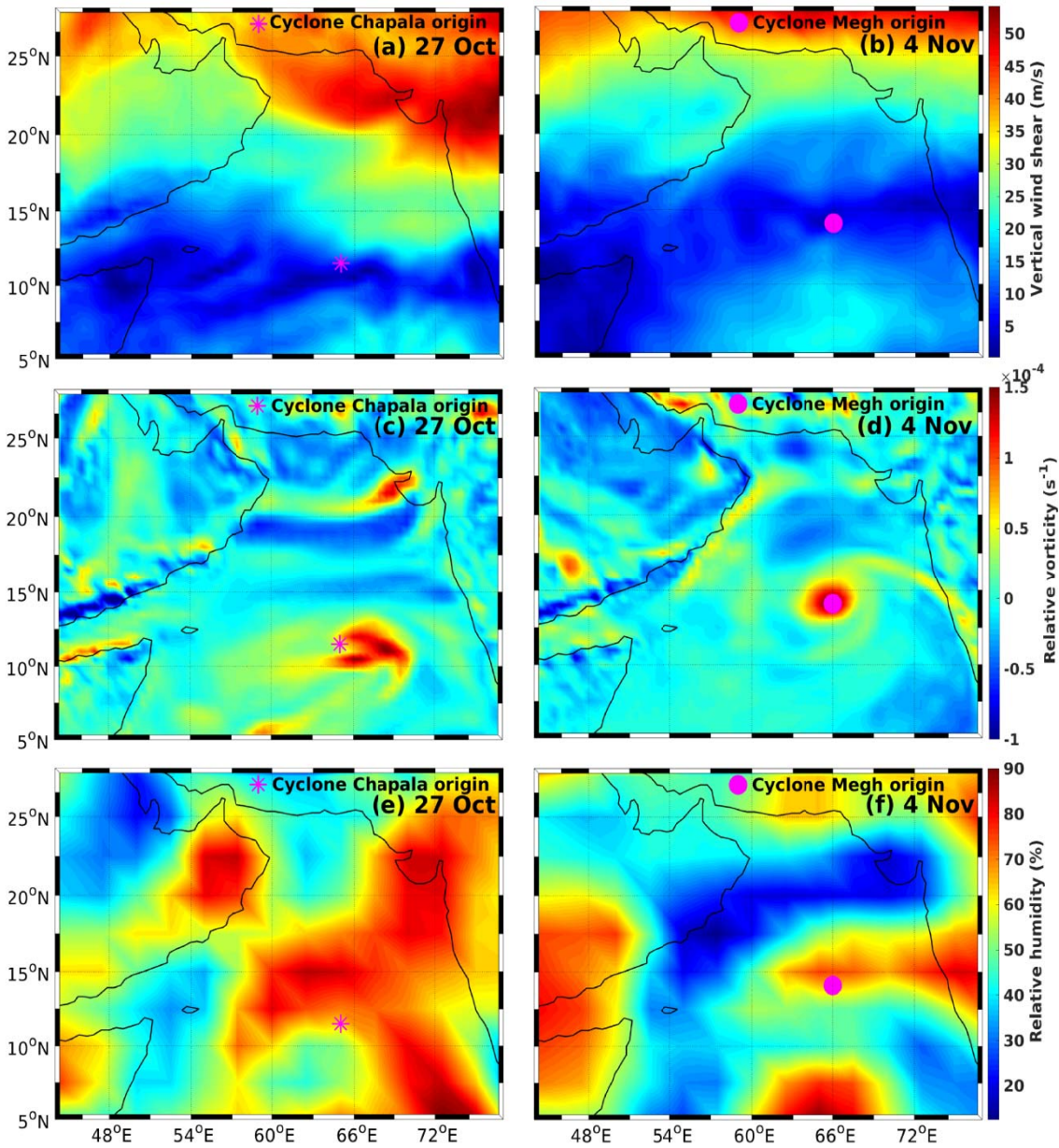


**Figure 7** Spatial distribution of (a,b) vertical wind shear between 200 and 850 hPa (m/s), (c, d) lower-tropospheric relative vorticity (850 hPa;  $s^{-1}$ ), and (e, f) mid-tropospheric relative humidity (500 hPa; %). The left panels (a, c, e) are for 27<sup>th</sup> October 2015 and right panels (b, d, f) are for 4<sup>th</sup> November 2015. The magenta filled asterisk and circle denote the location of origin of Chapala in left panels and Megh in the right panel respectively.



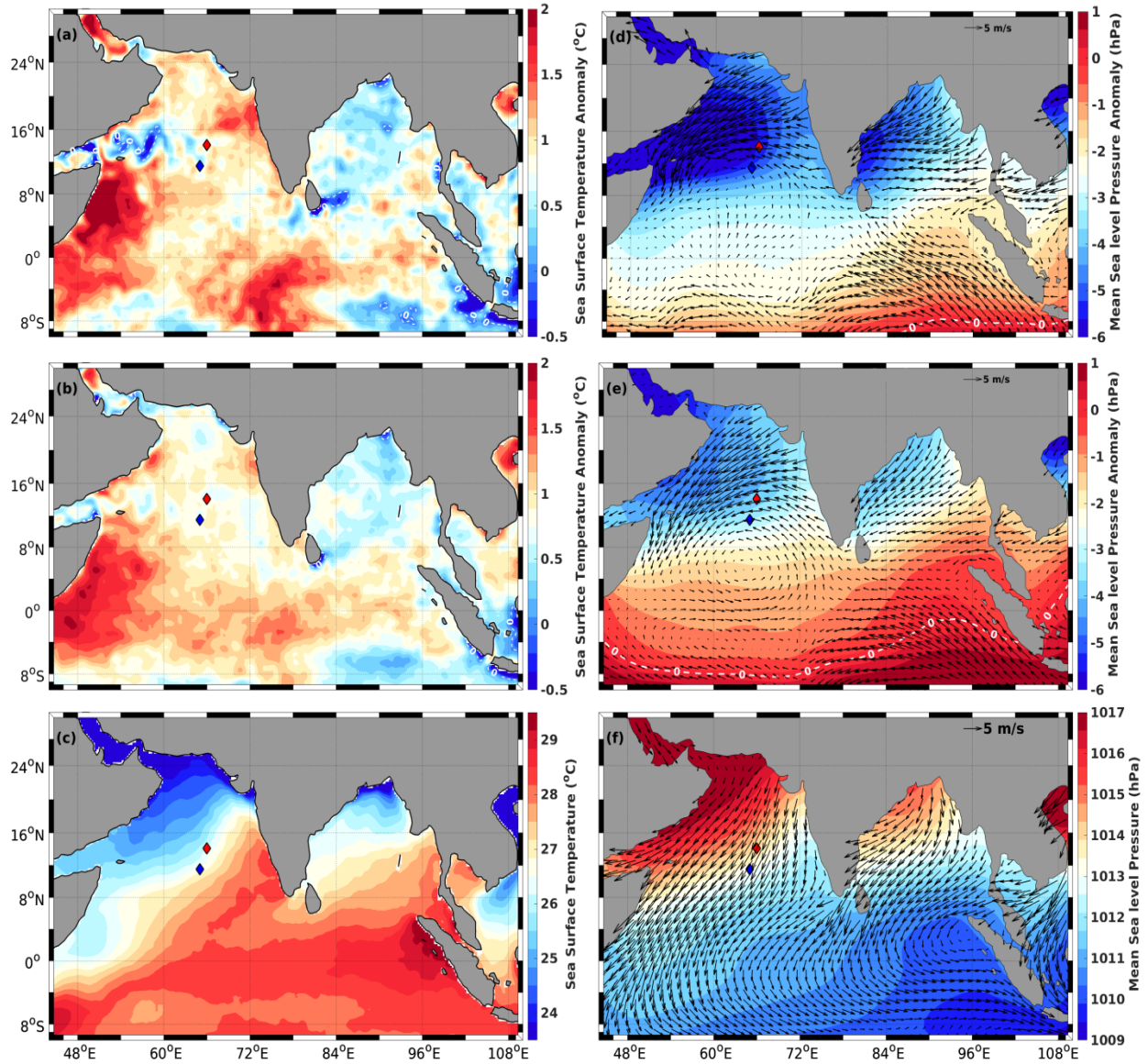


**Figure 8** Spatial distribution of SST anomaly and SST climatology (left panels) and sea level pressure (SLP) anomaly and SLP climatology (right panels) composited for (a, d) the cyclone period from 28<sup>th</sup> October to 10<sup>th</sup> November 2015, (b, e) composited for October-November 2015 (c, f) and October-November climatology. The white broken lines in (a), (b), (d) & (e) indicate the zero contours. The vectors overlaid in (d) & (e) are the sea surface wind anomaly, while that in (f) is the surface wind climatology. The filled blue and red diamonds are the locations of the origin of cyclones Chapala and Megh respectively.

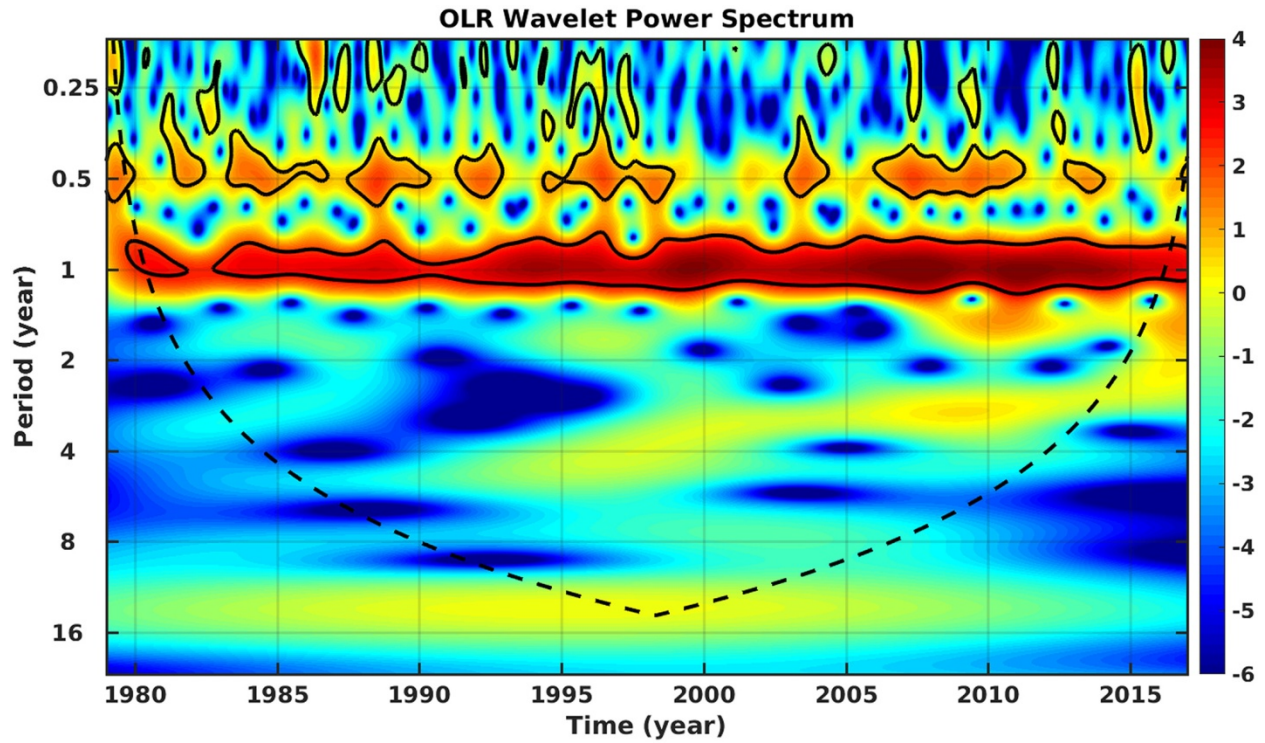


**Figure 9** Morlet wavelet power spectrum of monthly mean outgoing longwave radiation (OLR) for the period 1979-2017. The black broken line enclosing the conical region in the figure depicts the area where the signal is 95% significance.



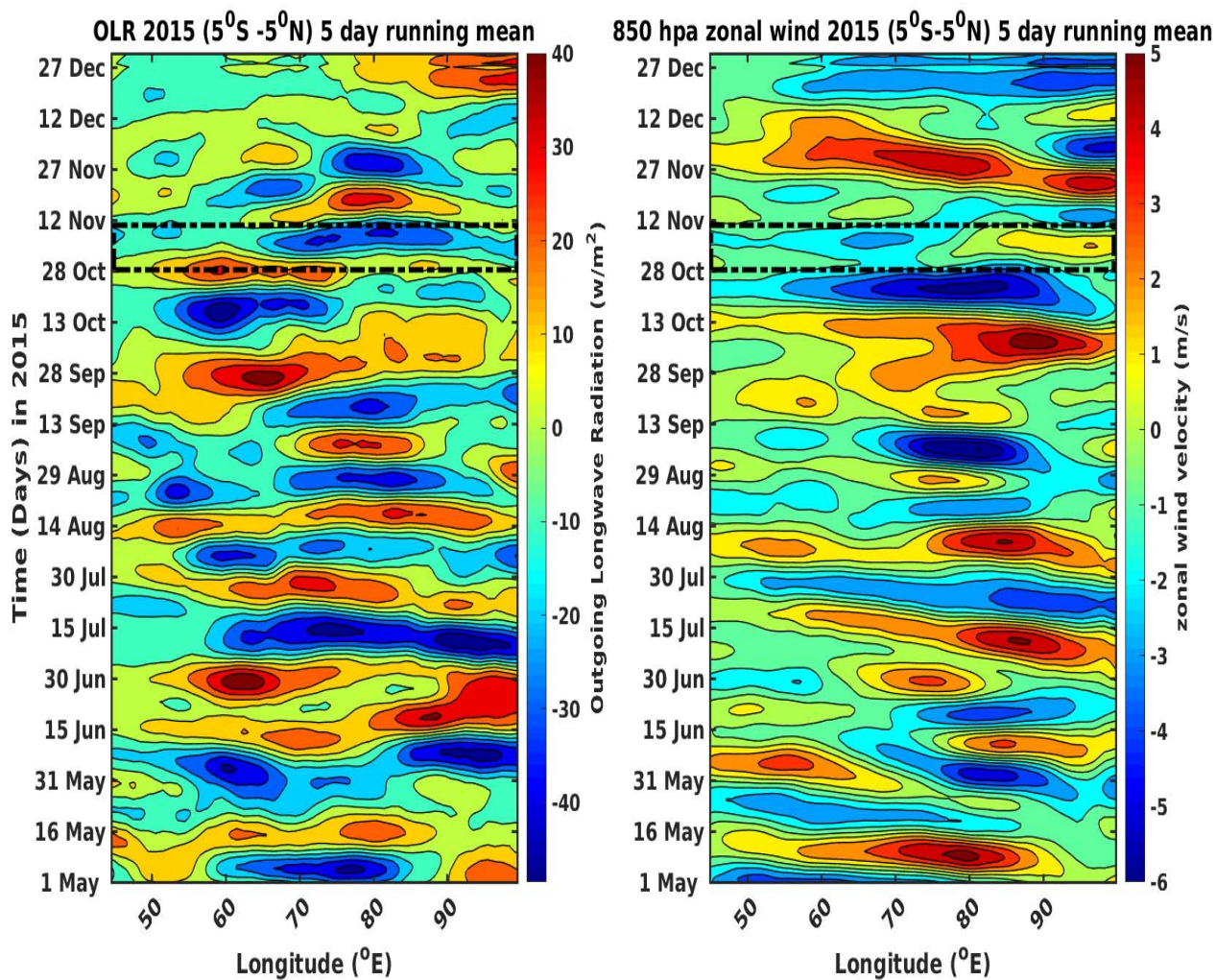


**Figure 10** Five-day running mean of (left panel) outgoing longwave radiation (OLR,  $w/m^2$ ) and (right panel) zonal wind (m/s) at 850 hPa averaged over  $5^\circ S$  to  $5^\circ N$  from  $44^\circ E$  to  $100^\circ E$  for the period 1<sup>st</sup> May to 31<sup>st</sup> December 2015. The horizontal black broken line indicates the period of the cyclones Chapala and Megh, while the slanting broken white line indicates the propagation of negative OLR (intense convection) and negative zonal wind (westerly winds).



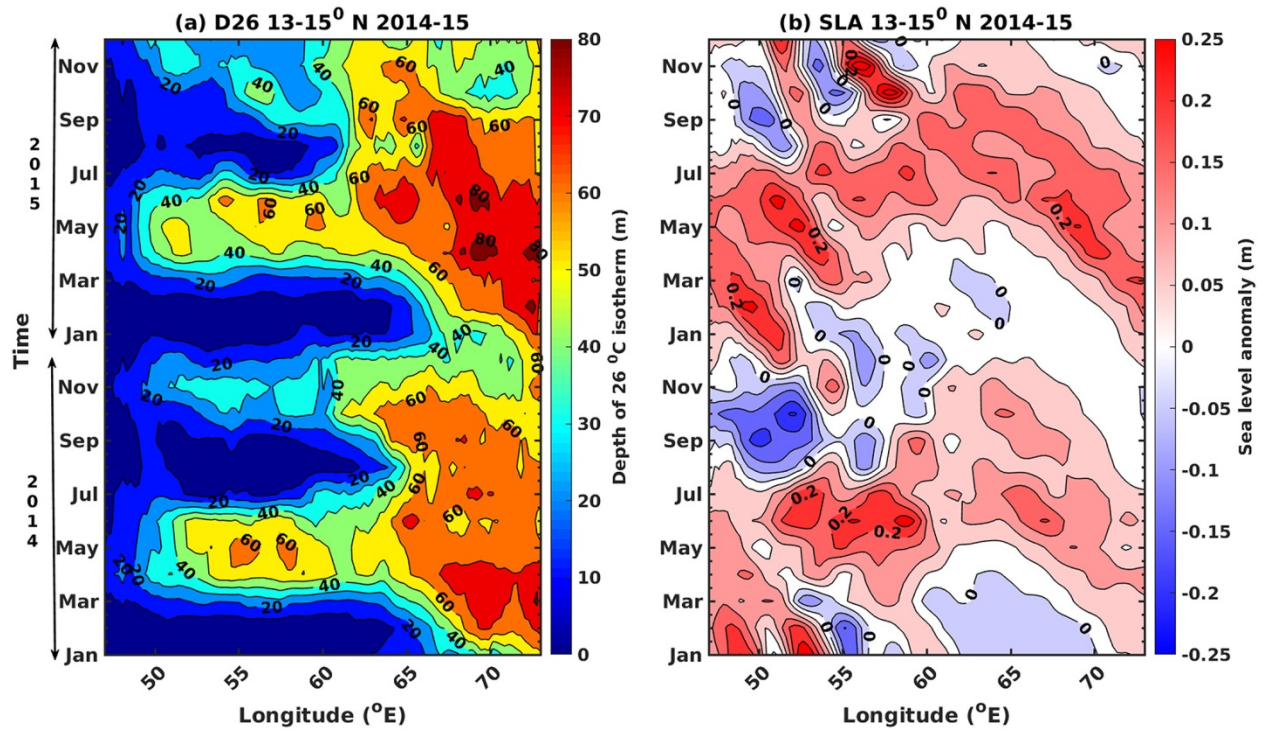


**Figure11** Monthly variation of (a) depth of 26°C isotherm (m) and (b) sea level anomaly (SLA, m) along 13-15°N from 48°E to 72°E in the Arabian Sea from January 2014 to December 2015.

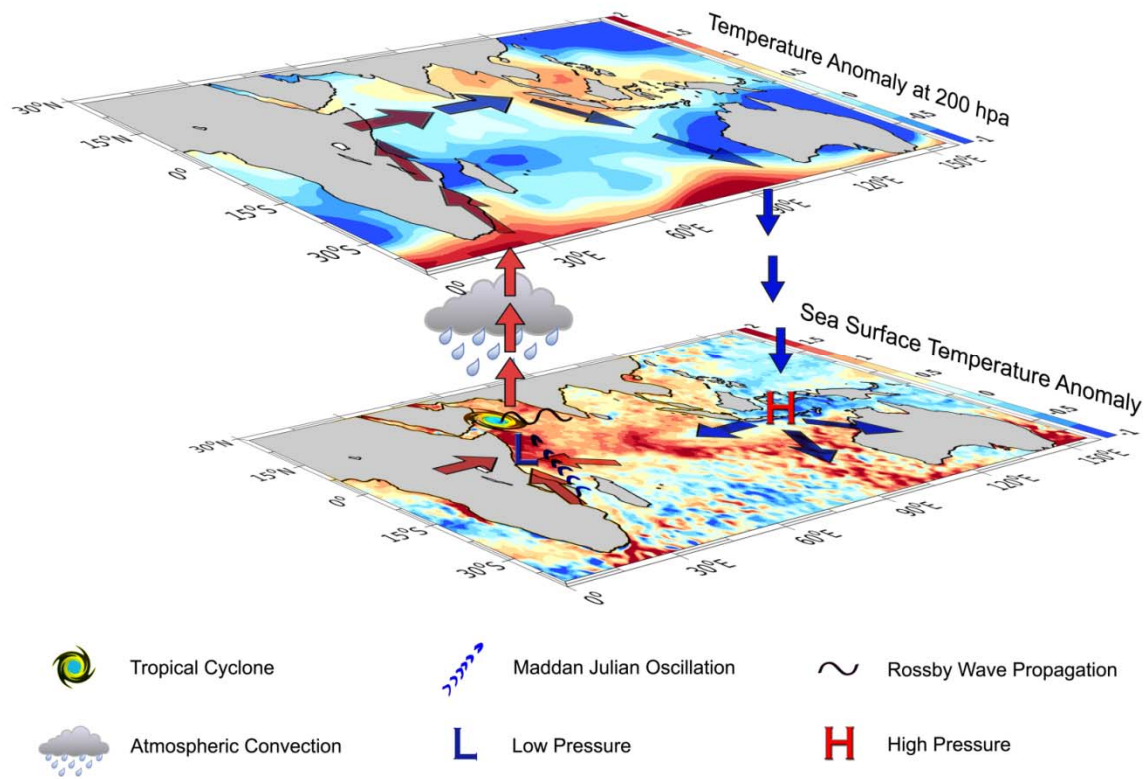


**Figure 12** Schematic diagram showing the process that led to the generation of back-to-back cyclones Chapala and Megh in the Arabian Sea during October-November 2015. See the text for details.